Atmos. Meas. Tech., 4, 1491–1514, 2011
www.atmos-meas-tech.net/4/1491/2011/
doi:10.5194/amt-4-1491-2011

Atmospheric Measurement Techniques

Operational total and tropospheric NO_2 column retrieval for GOME-2

P. Valks[1], G. Pinardi[2], A. Richter[3], J.-C. Lambert[2], N. Hao[1], D. Loyola[1], M. Van Roozendael[2], and S. Emmadi[1]

[1]Institut für Methodik der Fernerkundung (IMF), Deutsches Zentrum für Luft- und Raumfahrt (DLR), Oberpfaffenhofen, Germany
[2]Belgian Institute for Space Aeronomy, Brussels, Belgium
[3]Institute of Environmental Physics, University of Bremen, Germany

Received: 10 February 2011 – Published in Atmos. Meas. Tech. Discuss.: 9 March 2011
Revised: 4 July 2011 – Accepted: 11 July 2011 – Published: 26 July 2011

Abstract. This paper presents the algorithm for the operational near real time retrieval of total and tropospheric NO_2 columns from the Global Ozone Monitoring Experiment (GOME-2). The retrieval is performed with the GOME Data Processor (GDP) version 4.4 as used by the EUMETSAT Satellite Application Facility on Ozone and Atmospheric Chemistry Monitoring (O3M-SAF). The differential optical absorption spectroscopy (DOAS) method is used to determine NO_2 slant columns from GOME-2 (ir)radiance data in the 425–450 nm range. Initial total NO_2 columns are computed using stratospheric air mass factors, and GOME-2 derived cloud properties are used to calculate the air mass factors for scenarios in the presence of clouds. To obtain the stratospheric NO_2 component, a spatial filtering approach is used, which is shown to be an improvement on the Pacific reference sector method. Tropospheric air mass factors are computed using monthly averaged NO_2 profiles from the MOZART-2 chemistry transport model. An error analysis shows that the random error in the GOME-2 NO_2 slant columns is approximately 0.45×10^{15} molec cm^{-2}. As a result of the improved quartz diffuser plate used in the GOME-2 instrument, the systematic error in the slant columns is strongly reduced compared to GOME/ERS-2. The estimated uncertainty in the GOME-2 tropospheric NO_2 column for polluted conditions ranges from 40 to 80 %. An end-to-end ground-based validation approach for the GOME-2 NO_2 columns is illustrated based on multi-axis MAXDOAS measurements at the Observatoire de Haute Provence (OHP). The GOME-2 stratospheric NO_2 columns are found to be in good overall agreement with coincident ground-based measurements at OHP. A time series of the MAXDOAS and the GOME-2 tropospheric NO_2 columns shows that pollution episodes at OHP are well captured by GOME-2. Monthly mean tropospheric columns are in very good agreement, with differences generally within 0.5×10^{15} molec cm^{-2}.

Correspondence to: P. Valks
(pieter.valks@dlr.de)

1 Introduction

Nitrogen dioxide (NO_2) plays a key role in both stratospheric and tropospheric chemistry. In the stratosphere, it is involved in ozone destruction via a direct reaction with atomic oxygen and in the reaction cycles of halogen compounds (e.g. Solomon, 1999). In the troposphere, NO_2 is an important air pollutant affecting human health and ecosystems and one of the most important ozone precursors (e.g. Jacob et al., 1996; Seinfeld and Pandis, 1998). As a greenhouse gas, NO_2 contributes significantly to radiative forcing locally over industrial and urban areas. Although the direct contribution of tropospheric NO_2 to global warming is relatively small, emissions of nitrogen oxides ($NO_x = NO + NO_2$) also have an indirect effect on the global climate by perturbing ozone and methane concentrations. The main anthropogenic sources of nitrogen oxides are combustion of fossil fuels and biomass burning, the most important natural sources are microbial production in soils, wildfires and lightning. The industrialisation and population growth in the 19th and 20th century have resulted in a strong increase of the anthropogenic NO_x emissions since pre-industrial times. Although recently emissions have decreased in several industrialized countries (e.g. in Europe and North America) as a result of pollution

reduction measures, emissions in rapidly developing countries in Asia and elsewhere continue to increase. Studies using GOME and SCIAMACHY satellite measurements found especially strong increases in tropospheric NO_2 over China during the last decades (Richter et al., 2005; van der A et al., 2006, 2008).

Complementary to ground-based measurements, which provide accurate information on the local NO_2 concentrations, observations from space platforms offer the possibility to measure the distribution of NO_2 globally, including remote places with few in-situ measurements, and to study its large scale temporal and spatial variability. The Global Ozone Monitoring Experiment (GOME), launched on ERS-2 in 1995, provides NO_2 column amounts with a spatial resolution of $320 \times 40\,km^2$ and achieves global coverage within three days (Burrows et al., 1999). GOME data has been used to study the variation of stratospheric NO_2 and to monitor and investigate several important aspects of stratospheric chemistry and dynamics e.g. the Noxon-Cliff, zonal symmetry, or interhemispheric differences (Wenig et al., 2004). Several papers have been published on the retrieval of tropospheric NO_2 from GOME (e.g. Leue et al., 2001; Velders et al., 2001; Martin et al., 2002; Richter and Burrows, 2002). Over NO_2 source regions, such as Europe, South East Asia and North America, the tropospheric component of the NO_2 column is comparable in magnitude to the stratospheric component. Major challenges are involved in quantifying this tropospheric NO_2 column from satellite measurements involving the subtraction of the estimated stratospheric NO_2, and the conversion of the tropospheric residual into a vertical column using an accurate tropospheric air mass factor (Boersma et al., 2004).

A new generation of satellite instruments provides trace gases measurements with better spatial resolution that allow a detailed view of the NO_2 pollution patterns (Richter et al., 2005; Bucsela et al., 2006; Boersma et al., 2007). These are the Scanning Imaging Absorption Spectrometer for Atmospheric Chartography (SCIAMACHY) (Bovensmann et al., 1999) on the Envisat platform, the Ozone Monitoring Instrument (OMI) (Levelt et al., 2006) on EOS-Aura, and GOME-2 aboard MetOp-A (Callies et al., 2000; Munro et al., 2006). GOME-2, the subject of the current study, observes about 4 times smaller ground pixels than its predecessor GOME on ERS-2 and provides an almost global coverage on a daily basis. With the launch of GOME-2 on MetOp-A, the foundation was laid for a continuous data set of at least 25 yr of NO_2 measurements from space. Two more GOME-2 sensors on the MetOp-B and MetOp-C platforms will extend the GOME type data record until 2020. This unique data record will be further extended by the Sentinel-5 precursor to be launched by the middle of this decade, and the Sentinel-4 and Sentinel-5 sensors scheduled for the end of this decade.

In this paper, we describe the operational total and tropospheric NO_2 retrieval algorithms for GOME-2, as implemented in the GOME Data Processor (GDP) version 4.4 and developed within the framework of EUMETSAT's Satellite Application Facility on Ozone and Atmospheric Chemistry Monitoring (O3M-SAF). First, we give an overview of the GOME-2 satellite instrument, followed by a description of the near real time processing and data transport. Then the various steps in the total and tropospheric NO_2 column retrieval algorithms are presented. In Sect. 3, the NO_2 slant column retrieval using the differential optical absorption spectroscopy (DOAS) method is described and in Sect. 4, the air mass factor and the total vertical column computation are discussed. Section 5 describes the tropospheric NO_2 column retrieval and some examples of GOME-2's NO_2 monitoring capabilities are given. An error assessment of the GOME-2 NO_2 columns is presented in Sect. 6. The final part of this paper is devoted to a ground-based validation study of the operational GOME-2 NO_2 data product. The validation methodology is described and the end-to-end validation is illustrated using measurement results obtained at the Observatoire de Haute Provence (44° N, 5.7° E).

2 The GOME-2 instrument

The Second Global Ozone Monitoring Experiment (GOME-2) on the MetOp-A satellite, launched in October 2006, is part of the EUMETSAT Polar System (EPS). MetOp-A is flying on a sun-synchronous orbit with an equator crossing time of 09:30 local time (descending node) and a repeat cycle of 29 days. The GOME-2 instrument on MetOp continues the long-term monitoring of atmospheric trace gases, including O_3 and NO_2, started by GOME (launched on ESA's ERS-2 platform in 1995) and continued with SCIAMACHY (launched on ESA's ENVISAT platform in 2002). GOME-2 is an improved version of the GOME instrument on the ERS-2 satellite (see Table 1 and Callies et al., 2000; Munro et al., 2006). It is a nadir-scanning UV-VIS spectrometer with four main optical channels, covering the spectral range between 240 and 790 nm with a spectral resolution between 0.26 nm and 0.51 nm (FWHM). Additionally, two polarisation components are measured with polarisation measurements devices (PMDs) at 30 broad-band channels covering the full spectral range.

The default swath width of the GOME-2 scan is 1920 km, which enables global coverage in about 1.5 days. The along-track dimension of the instantaneous field of view is ∼40 km, while the across-track dimension depends on the integration time used for each channel. For the default 1920 km swath and the default integration time of 187.5 ms, the ground pixel size is $80 \times 40\,km^2$ (across-track × along-track) in the forward scan. Owing to a non-linear movement of the scan mirror, the ground pixel size remains nearly constant over the full scan.

GOME-2 measures the back-scattered and reflected radiation from the earth-atmosphere system. In addition, a direct sun spectrum is recorded once per day via a diffuser plate.

Table 1. Summary of GOME-2 instrument characteristics (Munro et al., 2006). The main improvements as compared to GOME/ERS-2 are shown in italic.

Principle	Nadir-scanning UV/VIS grating spectrometer
Wavelength range	240–790 nm in 4 channels *300–800 nm in 2 polarisation channels (s/p) with 15 bands*
Spectral sampling	0.12–0.21 nm (main channels)
Spectral resolution	*0.26–0.51 nm (FWHM)*
Swath width	*1920 km (default)*
Swath type	*Earth-curvature compensating*
Integration time	*187.5 ms (default)*
Spatial resolution	*80 × 40 km^2(default)*
Internal calibration	*Spectral lamp (PtCrNeAr), White lamp*, LED
Sun diffuser	*Quartz quasi-volume*

An important improvement of the GOME-2 instrument compared to GOME/ERS-2 is the use of a quartz quasi-volume diffuser for the direct sun measurements. The sun-angle dependent differential structures in the bi-directional scattering distribution function (BSDF) for this diffuser is strongly reduced compared the ground aluminium diffuser as used in GOME/ERS-2. The effect of the improved diffuser on the NO_2 slant column retrieval with GOME-2 is discussed in Sect. 6.1.

2.1 Data transport and processing

The operational GOME-2 total column NO_2 product is provided by the German Aerospace Center (DLR) in the framework of EUMETSAT's Satellite Application Facility on Ozone and Atmospheric Chemistry Monitoring (O3M-SAF). The focus of the O3M-SAF is to process, archive, validate and disseminate atmospheric data products of ozone, NO_2 and various other trace gases, aerosols and surface ultraviolet radiation.

The first step in the processing chain is the production of calibrated and geolocated level 1 radiances (level 0-to-1 processing). MetOp (level 0) data is transmitted once per orbit to the EUMETSAT ground station in Svalbard, Norway. Level 1 products are generated operationally in the Core Ground Segment (CGS) at EUMETSAT headquarters in Darmstadt, Germany and are broadcasted via the EUMETCast system in data chunks called PDUs, each containing 3 min of measurements.

The GOME-2 level 1 PDUs are received at the O3M-SAF processing facility in DLR, Germany, approximately 1 h and 45 min after sensing. The DLR multi-mission payload ground segment system (Heinen et al., 2009) controls the reception, processing, archiving, ordering and dissemination of the GOME-2 trace gas column products. The GOME-2 level 1 PDUs are processed with the UPAS (Universal Processor for UV/VIS Atmospheric Spectrometers) system, a new generation system for the processing of operational trace gas and cloud property products in near-real time and off-line (Livschitz and Loyola, 2003; Valks et al., 2011). The resulting GOME-2 level 2 products are disseminated through EUMETCast, WMO/GTS and the Internet. The level 1 data reception, processing with UPAS and level 2 data dissemination takes less than 15 min in total. The end user receives the GOME-2 level 2 near-real-time total column products in less than two hours after sensing with a committed service of 24 h a day, 365 days a year. DLR provides also offline and reprocessed GOME-2 level 2 consolidated products on an orbital basis. These can be ordered via the EUMETSAT product navigator (http://navigator.eumetsat.int) or DLR EOWEB systems (http://eoweb.dlr.de).

3 DOAS slant column fitting

The first major algorithm component in the NO_2 column retrieval with the GOME Data Processor (GDP) is the DOAS fitting (Platt, 1994; Platt and Stutz, 2008). This is a straightforward least-squares inversion to deliver the effective slant column of total NO_2, plus a number of auxiliary fitted parameters and error diagnostics. In DOAS fitting for optically thin absorbers, such as NO_2 in the visible wavelength region, the basic model is the Beer-Lambert extinction law. A polynomial closure term accounts for broadband effects: molecular scattering, aerosol scattering and absorption and reflection from the Earth's surface. We also include an additive spectrum for Ring effect interference (Chance and Spurr, 1997). The DOAS equation is then:

$$\ln\left[\frac{I(\lambda)}{I^0(\lambda)}\right] = -\sum_{\mathrm{g}} S_{\mathrm{g}}\sigma_{\mathrm{g}}(\lambda) - \sum_{j=0}^{3}\alpha_j\left(\lambda-\lambda^*\right)^{\mathrm{j}} - \alpha_{\mathrm{R}}R(\lambda) \quad (1)$$

Here, $I(\lambda)$ is the earthshine spectrum at wavelength λ, $I_0(\lambda)$ the daily reference (solar) spectrum, S_{g} the slant column density of gas g, and $\sigma_{\mathrm{g}}(\lambda)$ is the associated trace gas absorption cross section. The second term in Eq. (1) is the closure polynomial (a third-order polynomial has been assumed for the NO_2 retrieval), with λ^* a reference wavelength for this polynomial. The last term on the right hand side of Eq. (1) is the additive term for the Ring reference spectrum $R(\lambda)$. The fitting minimizes the weighted least squares difference between measurement based optical densities (on the left side of Eq. (1)) and simulated optical densities (on the right hand side of Eq. (1)). The DOAS-fit is linear in the slant columns S_{g}, the polynomial coefficients α_j and the Ring scaling parameter α_{R} (it becomes non-linear when shift and squeeze parameters are applied, as described below). The fitting window for NO_2 is 425–450 nm in GOME-2 Channel 3. In this wavelength region, the differential NO_2 absorption features

are prominent, the interference by other species is small, and GOME-2 measurements have a relatively high signal-to-noise ratio. For the reference spectrum, daily solar spectra measured with GOME-2 are used.

In the DOAS-fit, the absorption cross-section for NO_2 and O_3 from Gür et al. (2005) are used, which have been measured with the GOME-2 Flight Model (FM). The GOME-2 FM cross-sections were measured at five different temperatures (203, 223, 243, 273 and 293 K) under instrumental conditions of the in-flight operation aboard MetOp. An important advantage of these spectra is that the GOME-2 FM spectrometer is a well-characterized instrument including both spectral and radiometric calibration, and its instrumental line shape was accurately determined. DOAS analyses with GOME-2 data show that the Flight Model cross-sections provide consistent and stable fitting results in the NO_2 fitting window (Lambert et al., 2008).

The NO_2 absorption cross-section has a marked temperature dependence in this wavelength region, which has to be taken into account to improve the accuracy of the retrieved columns. In the DOAS fit, a single NO_2 cross-section reference spectrum at 243 K is used, and an a posteriori correction for the difference between the atmospheric temperature and the 243 K cross-sections temperature is performed on the air mass factor level (see Sect. 4).

Although the O_3 absorption in this part of the Chappuis band is weak (one reason for the fitting window choice), O_3 is included in the fit as interfering species (at 221 K). The other interfering species are O_2-O_2 and H_2O and their cross-sections are included in the fit as well. The inclusion of these interfering species in the fit reduces the uncertainty in the NO_2 slant column, especially for tropical areas (Lambert and Balis, 2004). Sources for the cross-section data are Greenblatt et al. (1990) for O_2-O_2 (wavelength axis recalibrated) and HITRAN 2000 (Rothman et al., 2003) for H_2O (the latter as input to line-by-line computations which are followed by convolution with the GOME-2 FM slit function).

The Ring effect (filling-in of well-modulated solar and absorption features in earthshine spectra) is due to inelastic rotational Raman scattering (RRS). In DOAS fitting, it is treated as an additional absorber, by means of an additive Ring reference spectrum and associated scaling parameter, as in Eq. (1) above. The "Fraunhofer" Ring spectrum is obtained by folding rotational Raman cross-sections at a fixed temperature with a high-resolution Fraunhofer spectrum taken from the Kitt Peak Observatory (Chance and Spurr, 1997). This does not include a telluric contribution (molecular Ring effect), but for NO_2 the error in the retrieved total column due to the molecular Ring effect is small (1–2 %) as compared to the other error sources.

Intensity offset effects that may be induced by residual spectral stray-light, inelastic scattering in the atmosphere and the ocean or remaining calibration issues in the GOME-2 level-1 product are known to be possible sources of bias in DOAS retrievals of minor trace species; to partly correct for possible offset the inverse of the sun spectrum is fitted as another effective cross-section (Platt and Stutz, 2008).

Shift and squeeze parameters may be applied to cross-section wavelength grids to improve wavelength registration against level-1 spectra or compensate for inaccuracies in the wavelength calibration of the cross-section data. Experience with DOAS in the operational UPAS system has shown that fitting of such non-linear parameters on a pixel-by-pixel basis can sometimes lead to numerical instability, and an optimized pre-shift value needs to be applied (Lambert et al., 2002). For GOME-2, an optimized pre-shift value of -0.022 nm is applied to the Flight Model NO_2 cross-sections.

In the GDP 4.4, the solar spectrum is used as the wavelength reference. Shift and squeeze parameters are fitted for each Earthshine spectrum to compensate for the Doppler shift and changing thermal stress. If necessary, the wavelength calibration of the GOME-2 level-1 spectra can be improved by applying window-dependent pre-shifts to parts of the solar spectrum before each orbit of data is processed. These pre-shifts are established by cross-correlation with a high-resolution solar spectrum (Chance and Spurr, 1997) over limited wavelength ranges covering the fitting window (i.e. 425–450 nm for NO_2 and 758–772 nm covering the oxygen A-band as used in the ROCINN cloud algorithm).

4 Air mass factor and initial total VCD computations

The second component in the retrieval is the conversion of the NO_2 slant column density into the vertical column density (VCD) V, using the air mass factor M:

$$M = \frac{S}{V} \tag{2}$$

The air mass factor depends on the vertical NO_2 profile and a set of forward model parameters $\boldsymbol{b}$, including the GOME-2 viewing geometry, surface albedo, clouds and aerosols. For optically thin absorbers, such as NO_2 in the visible wavelength region, the radiative transfer calculations can be decoupled from the trace gas profile shape (Palmer et al., 2001):

$$M = \frac{\sum_l m_l(\boldsymbol{b}) x_l c_l}{\sum_l x_l} \tag{3}$$

where m_l is the air mass factors for the individual layer l (independent of the NO_2 profile), and x_l the partial NO_2 column in layer l. The altitude-dependent air mass factors m_l are calculated with the LIDORT radiative transfer model (Spurr et al., 2001), as described in Sect. 4.1. The coefficients c_l are layer-specific correction factors that account for the temperature dependence of the NO_2 absorption cross-section. This correction factor is a function of the atmospheric temperature in layer l and the fixed temperature (243 K) of the NO_2 absorption cross-sections assumed in the DOAS fit (Boersma et al., 2004; Nüß et al., 2006). In the

GDP 4.4 algorithm, monthly mean temperatures taken from a run of the MOZART-2 model (see Sect. 5.2) are used to calculate the correction factors for the tropospheric layers.

The initial total VCD is computed under the assumption that the troposphere is not polluted. Therefore, the air mass factor is based on stratospheric NO_2 profiles only, whereas the tropospheric NO_2 amount is assumed to be negligible. This approach is valid over large parts of the Earth, but in areas with significant tropospheric NO_2, the total column densities are underestimated and need to be corrected, as described in Sect. 5.2.

To incorporate the seasonal and latitudinal variation in stratospheric NO_2 in the air mass factor calculations, a harmonic climatology of stratospheric NO_2 profiles is used (Lambert et al., 2000). This harmonic climatology has been derived from satellite measurements by UARS/HALOE (Gordley et al., 1996) and SPOT-4/POAM-III (Randall et al., 1998) and complementary information from ground-based measurements from the Network for the Detection of Atmospheric Composition Change (NDACC). The stratospheric NO_2 profiles are time dependent and given for 16 latitude bands. Latitude and time of GOME-2 measurements are specified from level-1b geolocation information. In order to avoid jump artefacts associated with discrete latitude classifications, the climatological profiles are interpolated between latitude bands using a linear weighting scheme based on the cosine of the latitude (to account for surface area differences). The resulting NO_2 concentration profile is then integrated to partial columns (x_l) on the layer grid of the radiative transfer model. For stratospheric air mass factor calculations, the vertical resolution does not need to be very high, and it is sufficient to use a 13-layer grid based on Umkehr layers.

For GOME-2 scenarios in the presence of clouds, the air mass factor can be determined in conjunction with GOME-2 derived cloud information using a Lambertian reflecting boundary cloud model and the independent pixel approximation (IPA):

$$M = (1-w)M_{\text{clear}} + w\,M_{\text{cloud}}, \tag{4}$$

where M_{clear} is the air mass factor for a completely cloud free pixel,M_{cloud} the air mass factor for a completely cloudy pixel, and w the cloud radiance fraction. M_{clear} and M_{cloud} are obtained with Eq. (3), with clouds treated as Lambertian equivalent reflectors and M_{cloud} calculated with $m_l = 0$ for all layers below the cloud-top pressure (p_c).

The cloud radiance fraction w is defined as:

$$w = \frac{c_f I_{\text{cloud}}}{(1-c_f)I_{\text{clear}} + c_f I_{\text{cloud}}}, \tag{5}$$

where c_f is the cloud fraction, I_{clear} and I_{cloud} are the backscattered radiances for cloud-free and cloud-covered scenes respectively. I_{clear} and I_{cloud} are calculated for the mid-point wavelength of the fitting window (437.5 nm) with the LIDORT radiative transfer model, and depend mainly on the surface and cloud albedos and on the GOME-2 viewing geometry.

4.1 Radiative transfer calculations

LIDORT is a multiple scatter multi-layer discrete ordinate radiative transfer code (Spurr et al., 2001). In LIDORT, the atmosphere is assumed to be stratified into a number of optically uniform layers. The LIDORT code used here neglects light polarisation. For DOAS retrievals in the visible wavelength range, the polarisation signature is small and subsumed in the closure polynomial. We use the LIDORT Version 3.3, which possesses corrections for beam attenuation along curved line-of-sight paths, needed for the wide viewing angles of GOME-2 (scan angles in the range 40–50°) (Spurr, 2008).

For DOAS applications with optically thin absorbers, such as NO_2 in the visible wavelength region, the trace gas air mass factor wavelength dependence is weak and therefore it is sufficient to use the mid-point wavelength of the fitting window (437.5 nm).

LIDORT is a scattering formalism, and requires as input the following optical properties in each layer: (1) total extinction optical thickness, (2) total single scattering albedo, and (3) total phase function scattering coefficients. LIDORT also requires knowledge of the surface reflection (assumed to be Lambertian). In the GDP 4.4, there is an "atmospheric/surface setup module" which deals with detailed radiative transfer physics of molecules, trace gases, aerosols, clouds and surface reflection as needed to create the necessary LIDORT inputs. This setup function is completely decoupled from LIDORT, and this gives the air mass factor computation great flexibility. It is straightforward to change input climatology and other reference atmospheric and surface datasets.

The climatology used for the surface albedo (including mean snow and ice cover) is derived from TOMS and GOME Lambert-equivalent reflectivity (LER) measurements at 380 and 440 nm, as described in Boersma et al. (2004). These monthly averaged surface albedo maps have a spatial resolution of $1° \times 1.25°$ and represent climatological (monthly) mean situations. The surface albedo for each GOME-2 pixel is determined via area-weighted tessellation of the climatological surface albedo maps and linear interpolation in time to the measurement day.

Changes in surface albedo values will chiefly affect the clear-sky air mass factor M_{clear} and the intensity-weighted cloud fraction w. The effect on the total and tropospheric NO_2 column is largest for cloud-free and partly cloudy scenes; for completely cloud-covered scenes the effect is generally small, since M_{clear} plays no part in the total NO_2 column calculations (see Eq. (4) with $w = 1$).

In addition to the albedo, the surface altitude is an important input for the air mass factor calculations, especially in the vicinity of mountainous terrain (Zhou et al., 2009).

To determine an accurate pixel-average surface altitude, the high resolution ($\sim 1 \times 1$ km) topography heights from the global digital elevation model GTOPO30 (http://lpdaac.usgs.gov/gtopo30/gtopo30.asp) are averaged over each GOME-2 pixel.

4.2 Cloud parameters

In the independent pixel approximation, clouds are regarded as reflecting Lambertian surfaces and cloud information is reduced to the specification of 3 parameters: cloud fraction, cloud-top albedo and cloud-top pressure. In the GDP 4.4, the OCRA and ROCINN algorithms (Loyola et al., 2007) are used for obtaining GOME-2 cloud information: OCRA provides the cloud fraction using the broad-band polarization measurements, and ROCINN provides cloud-top height and cloud-top albedo from measurements in and adjacent to the oxygen A-band around 760 nm. Being sensitive to light scattering by clouds, OCRA is also sensitive to scattering by aerosols present in a given GOME-2 scene (see Sect. 6.3). Note that the cloud model used in the NO_2 retrieval as described above is consistent with the cloud model used in the OCRA/ROCINN cloud retrieval, in the sense that both use the independent pixel approximation representing clouds as opaque Lambertian surfaces (Antón and Loyola, 2011).

With GOME-2, several improvements have been incorporated in the cloud algorithms. The initial ROCINN algorithm was based on transmittance-only calculations in the oxygen A-band. ROCINN version 2.0, as used for GOME-2, is based on radiative transfer simulations with Rayleigh scattering and polarization. Another important upgrade for GOME-2 is the ability to distinguish clouds in measurements affected by ocean surface sun-glint, a phenomenon that is common at the edges of the GOME-2 swath. OCRA discriminates clouds in the region affected by sun-glint by analysing the broad-band polarization measurements (Loyola et al., 2011).

5 Tropospheric NO_2 column algorithm

In this section, the retrieval of the tropospheric NO_2 column is presented. The tropospheric NO_2 column algorithm for GOME-2 consists of the following steps: (1) calculation of the initial total NO_2 column as described above, (2) estimation of the stratospheric component of the NO_2 column using a spatial filtering approach and (3) the conversion of the residual tropospheric slant column into a tropospheric vertical column, using an accurate tropospheric air mass factor (including the effects of clouds). In addition, the initial total NO_2 column is corrected for the tropospheric component under polluted conditions, to provide a more accurate total vertical column. A description of these algorithm steps is given below.

5.1 Stratospheric correction

After the calculation of the initial total NO_2 column, the next step in the retrieval of the tropospheric NO_2 column is the estimation of the stratospheric component from the initial total VCD. Most methods for the stratosphere-troposphere separation reported in the literature are based on the observation that stratospheric NO_2 has a smooth spatial behaviour and that tropospheric contributions occur near source regions on smaller geographic scales. The "Pacific Reference Sector" method has been used in several studies (e.g. Richter and Burrows, 2002; Martin et al., 2002; Beirle et al., 2003) and rests on the assumption of a longitudinally homogeneous stratospheric NO_2 layer and negligible tropospheric NO_2 over the Pacific. The stratospheric NO_2 column can then be derived as the average of the total VCD for each latitude over the longitude band in the Pacific sector. The first assumption is reasonable at lower latitudes, since NO_2 in the stratosphere is mainly determined by day length (photolysis of reservoir species) and only to a lesser degree by transport, ozone concentrations, and temperature. However, longitudinal variations cannot be neglected at higher latitudes, because of the dynamical variability, especially in winter and spring. To reduce the uncertainties involved in the stratosphere-troposphere separation at mid and high-latitudes, a spatial filtering method is employed for GOME-2 in the GDP 4.4. Various spatial filtering methods have been developed that use data not only from the Pacific, but also from other relatively clean areas to determine the stratospheric NO_2 column (Leue et al., 2001; Wenig et al., 2004; Bucsela et al., 2006). The spatial filtering procedure used here works as follows. First a global map is constructed from the initial NO_2 columns by binning the last 24 hours of GOME-2 data on a spatial grid of 2.5° latitude × 2.5° longitude. To minimize tropospheric biases in the stratospheric field, a global mask is applied to eliminate areas with potentially high amounts of tropospheric NO_2. This pollution mask is derived from MOZART-2 model results: the areas in the model with monthly mean tropospheric NO_2 columns larger than 1.0×10^{15} molec cm^{-2} are masked as polluted (see next section).

After pollution masking, the stratospheric NO_2 column is determined by low-pass filtering the initial NO_2 columns in the zonal direction (30° boxcar filter). This is done in two steps, where first the unmasked measurements with initial total VCD exceeding the (preliminary) stratospheric NO_2 column by more than one standard deviation are identified and excluded from the final analysis. Unmasked polluted measurements can occur when pollution events are missed by the model, for instance during transient pollution events. Finally, the stratospheric NO_2 is interpolated between latitude bands in order to avoid jump artefacts associated with a discrete latitude grid.

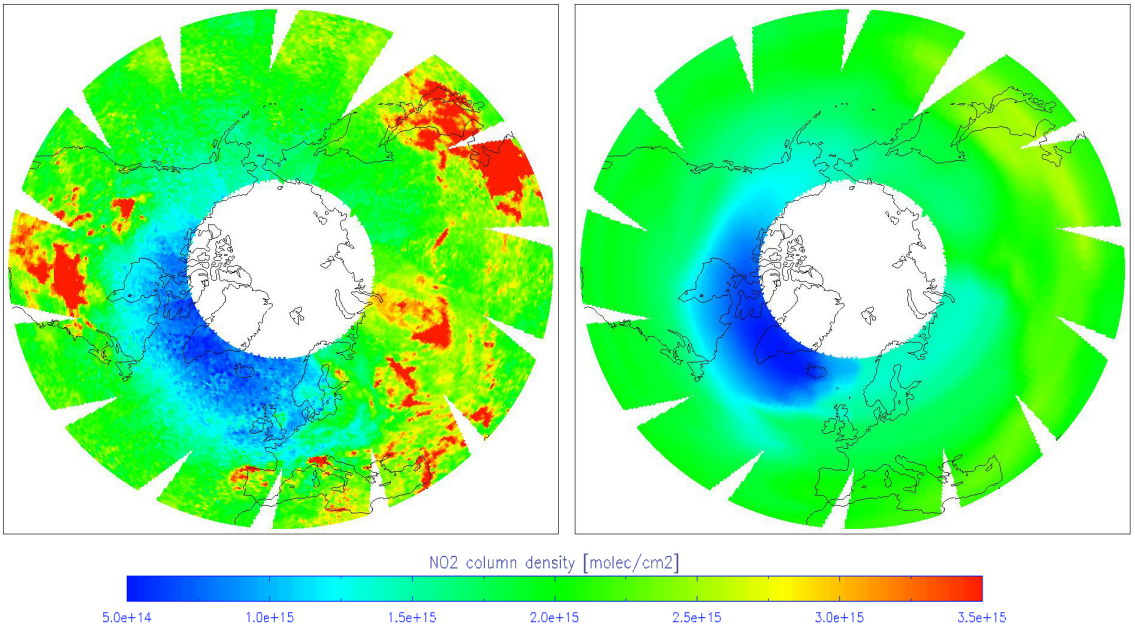

Fig. 1. Total NO_2 distribution from GOME-2 for 22 February 2008 (left) and the corresponding stratospheric NO_2 distribution as obtained with the spatial filtering approach (right).

A limitation of the spatial filtering approach used here is that it will also take up background NO_2 in the free troposphere with smooth spatial behaviour. In the GDP 4.4, a simple correction is applied for this effect: a fixed background NO_2 column (0.1×10^{15} molec cm^{-2}) is subtracted from the derived vertical stratospheric NO_2 column. This offset for the background NO_2 column has been derived from tropospheric NO_2 fields for the (unpolluted) Pacific region, as provided by the MOZART-2 model.

An example of the stratospheric NO_2 distribution obtained with the spatial filtering approach used in the GDP 4.4 is plotted in Fig. 1. This figure shows the initial total and stratospheric NO_2 columns from GOME-2 for the northern mid- and high-latitudes on 22 February 2008. Clearly visible in this figure are the longitudinal variations in stratospheric NO_2. The low values over the north polar area around Greenland and Eastern Canada indicate denoxified air masses inside the polar vortex. Due to dynamical variability, the location of these air masses can vary strongly within a time scale of a few days. Figure 1 shows that a large part of the area over the northern Atlantic with low NO_2 is captured by the spatial filtering approach on this day (which would not have been possible with the Pacific Reference Sector method). However, the stratospheric NO_2 column over parts of Northwestern Europe is overestimated by the stratospheric correction procedure, which results in an underestimation of the tropospheric NO_2 column. The uncertainty in the stratospheric column calculation is discussed in more detail in Sect. 6.2.

5.2 Tropospheric Air Mass Factor and VCD computation

After the stratosphere-troposphere separation, the tropospheric VCD can be determined via the relation:

$$V_t = \frac{S - M_s\, V_s}{M_t} \tag{6}$$

where S is the slant column density calculated in the DOAS fit and V_s is the stratospheric component, as calculated with the spatial filtering method described above. M_s is the stratospheric air mass factor, used for the calculation of the initial total VCD, as described in Sect. 4. M_t is a tropospheric air mass factor calculated with Eqs. (3) and (4), using an a priori tropospheric NO_2 profile. The tropospheric air mass factor depends on the same forward model parameters as the stratospheric air mass factor (i.e. GOME-2 viewing geometry, surface albedo, clouds and aerosols). However, the dependence on the surface albedo, clouds and aerosols, as well as the a priori NO_2 profile is much stronger for the tropospheric air mass factor. The variability in the tropospheric air mass factor is illustrated in Fig. 2. where a global map of the monthly averaged air mass factor is shown for March 2008. Small tropospheric air mass factors between 0.5 and 1.0 are found over polluted source regions, such as Europe, the Eastern US and Southeast Asia. Over unpolluted regions, like the oceans or the Sahara, and over snow covered areas the air mass factor is larger than 2.0.

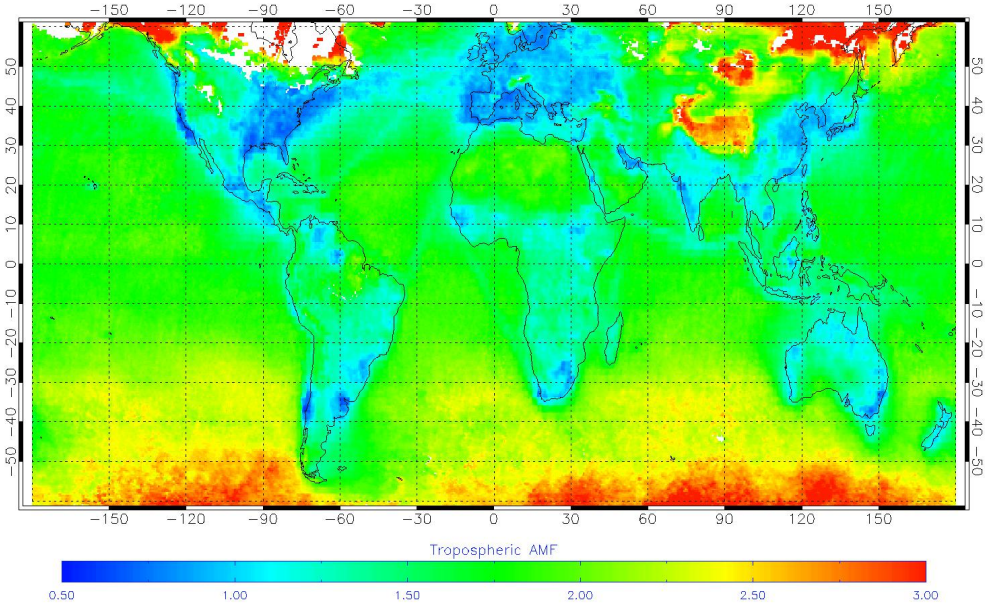

Fig. 2. Monthly averaged tropospheric air mass factors for March 2008, as calculated with the GDP 4.4.

After the calculation of the tropospheric column, a corrected total VCD V_c can be calculated via the relation:

$$V_c = V_s + V_t \quad (7)$$

In the GDP 4.4, a corrected total VCD is determined for all GOME-2 observations where the initial total VCD exceeds the estimated stratospheric component V_s.

The a priori NO_2 profiles used in GDP 4.4 are obtained from a run of the global chemistry transport model (CTM) MOZART version 2 (Horowitz et al., 2003). The model data has a horizontal resolution of 1.875° latitude by 1.875° longitude (T63), with 32 terrain-following hybrid layers extending from the surface up to ∼3 hPa. The number of layers in the troposphere varies from 10 to 16, depending on tropopause height, with about 4 layers in the boundary layer. For the tropospheric air mass factor computation in the GDP 4.4, monthly average profiles at the satellite overpass time have been determined, using MOZART-2 data from the year 1997 (Nüß et al., 2006). While this climatology will capture seasonal and spatial patterns and provides a good first guess of the atmospheric NO_2 profile, daily data from an online model run can capture short-term variability induced by meteorology and would therefore be preferable (Boersma et al., 2004). This option is currently under consideration for future versions of the GDP.

The calculation of the tropospheric VCD is complicated in case of (partly) cloudy conditions. For many measurements over cloudy scenes, the cloud-top is well above the NO_2 pollution in the boundary layer, and when the clouds are optical thick, the enhanced tropospheric NO_2 concentrations cannot be detected by GOME-2. Therefore, the tropospheric VCD is only calculated for GOME-2 observations with a cloud radiance fraction $w < 50$ %. Note that the "below cloud amount" (i.e. the amount of NO_2 that is inferred to be below the cloud top) for these partly cloudy conditions is implicitly accounted for via the cloudy air mass factor M_{cloud} (in which $m_l = 0$ for all layers below the cloud-top). As this procedure assumes knowledge of the vertical NO_2 profile (taken from the model) and neglects any possible differences of this profile in the cloudy and cloud-free part, cloudy scenes will have higher uncertainty than clear sky observations. There are several atmospheric processes that can result in differences between the NO_2 profiles in adjacent cloudy and clear scenes. Differences in the photolysis rates within and below clouds leads to changes in the NO/NO_2 ratio as well as in the OH concentrations which determines NO_2 removal. Both effects tend to increase NO_2 below a cloud relative to a similar cloud-free scene. In case of convective clouds, the vertical movement of air with updrafts in the centre of convection and downward movement of air at the sides can lead to significant changes of the vertical distribution of NO_2 over polluted regions. In clouds with lightning, the NO_2 produced in the middle and upper part of the cloud changes the vertical profile of NO_2 as well.

5.3 Examples of GOME-2 tropospheric NO_2

Figure 3 (left) shows the yearly averaged tropospheric NO_2 column from GOME-2 for 2007 over Europe, as retrieved with the GDP 4.4 algorithm described above. For comparison, the GDP 4.4 algorithm has been applied to GOME/ERS-2 data as well, and the results for 2000 are shown in Fig. 3 (right) (due to limited spatial coverage of the GOME measurements after June 2003, the tropospheric NO_2 algorithm

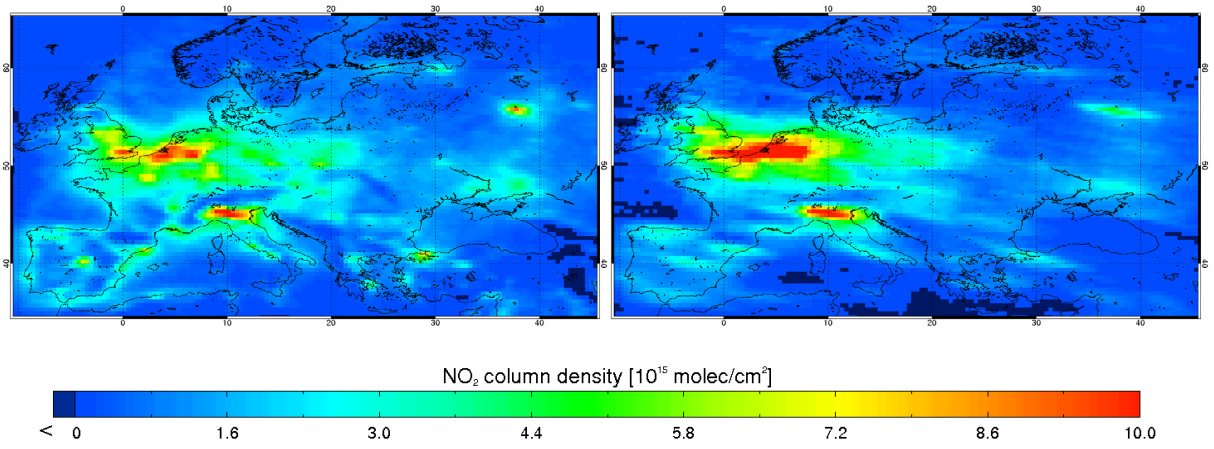

Fig. 3. Yearly average tropospheric NO_2 columns over Europe measured by GOME-2 for 2007 (left) and by GOME/ERS-2 for 2000 (right).

cannot be applied on more recent GOME measurements). Both panels show the high tropospheric NO_2 concentrations above large urban and industrial areas of Europe, such as the Po Valley, the Benelux, South-East England and Germany's Ruhr area. However, the better spatial coverage and resolution of GOME-2 compared to GOME/ERS-2 results in more spatial detail in the tropospheric NO_2 field (for the region shown in Fig. 3, there are about 6.5×10^5 GOME-2 measurements with a cloud radiance fraction $<50\,\%$ available, while the number of GOME/ERS-2 measurements is only $\sim 5 \times 10^4$). The increase in spatial detail is clearly visible in, for example, the "city-size" polluted areas around Paris, Madrid and Moscow, which are much better resolved in the GOME-2 panel.

Differences between GOME and GOME-2 tropospheric NO_2 fields are expected for several reasons. Better spatial resolution leads to larger NO_2 columns over pollution hotspots. Changes in NO_x emissions are expected to lead to lower NO_2 values in some countries while increases have been reported for others (Konovalov et al., 2010). When comparing GOME-2 and GOME/ERS-2 measurements, the diurnal variation in tropospheric NO_2 should be taken into consideration as well. There is a one hour difference between the local overpass time of GOME-2 ($\sim$09:30 LT) and GOME/ERS-2 ($\sim$10:30 LT). For the polluted regions in the European area, 5–10 % larger tropospheric NO_2 columns are expected at the earlier GOME-2 overpass time than at the GOME/ERS-2 overpass time (Boersma et al., 2008).

Figure 4 (left) shows the averaged tropospheric NO_2 columns from GOME-2 for the period 2007–2009 over East Asia. The world's largest area with high NO_2 pollution is found above east China, which is a result of China's spectacular economic growth during the last decade, accompanied by a strong increase in emissions of air pollutants. Another remarkable feature visible in the Fig. 4 is the enhanced tropospheric NO_2 along shipping lanes in the Bay of Bengal and the South China Sea (e.g. see Beirle et al., 2004; Franke et al., 2009; Richter et al., 2004, 2011). For comparison, the results for GOME/ERS-2 for the period 1997–1999 are also shown in Fig. 4 (right). The increased spatial detail of GOME-2 compared to GOME/ERS-2 is clearly visible. For example, the polluted areas around the large cities in Northern India, and around Bangkok are much better resolved in the GOME-2 panel. Also clearly visible is the increase in tropospheric NO_2 over Eastern China during the ten year period that lies between the two pictures, as a result of strong increased in NO_2 emissions (Richter et al., 2005; Van der A et al., 2008).

6 Error and sensitivity analyses

Referring to Eq. (6), the overall error on the tropospheric NO_2 column V_t (denoted as σ_{V_t}) can be expressed as a function of the error on the slant column density S, the stratospheric column V_s, and the stratospheric and tropospheric air mass factors M_s and M_t:

$$\begin{aligned}\sigma_{V_t}^2 &= \left(\frac{\partial V_t}{\partial S}\right)^2 \sigma_S^2 + \left(\frac{\partial V_t}{\partial V_s}\right)^2 \sigma_{V_s}^2 + \left(\frac{\partial V_t}{\partial M_s}\right)^2 \sigma_{M_s}^2 + \left(\frac{\partial V_t}{\partial M_t}\right)^2 \sigma_{M_t}^2 \\ &= \left(\frac{1}{M_t}\right)^2 \sigma_S^2 + \left(\frac{M_s}{M_t}\right)^2 \sigma_{V_s}^2 + \left(\frac{V_s}{M_t}\right)^2 \sigma_{M_s}^2 + \left(\frac{S - M_s V_s}{M_t^2}\right)^2 \sigma_{M_t}^2\end{aligned} \quad (8)$$

This assumes that the errors are independent and therefore can be treated with standard error propagation. While this is not always the case and systematic errors also contribute to the overall uncertainty, this approach will provide a rough estimate of the uncertainties to be expected. In the following sections, the error components from the slant column density σ_S, the stratospheric column σ_{V_S}, and the air mass factors σ_{M_s} and σ_{M_t} are discussed in more detail.

6.1 Uncertainty in the slant column density

The precision of the NO_2 slant column densities is derived from a statistical analysis of the GOME-2 measurements in

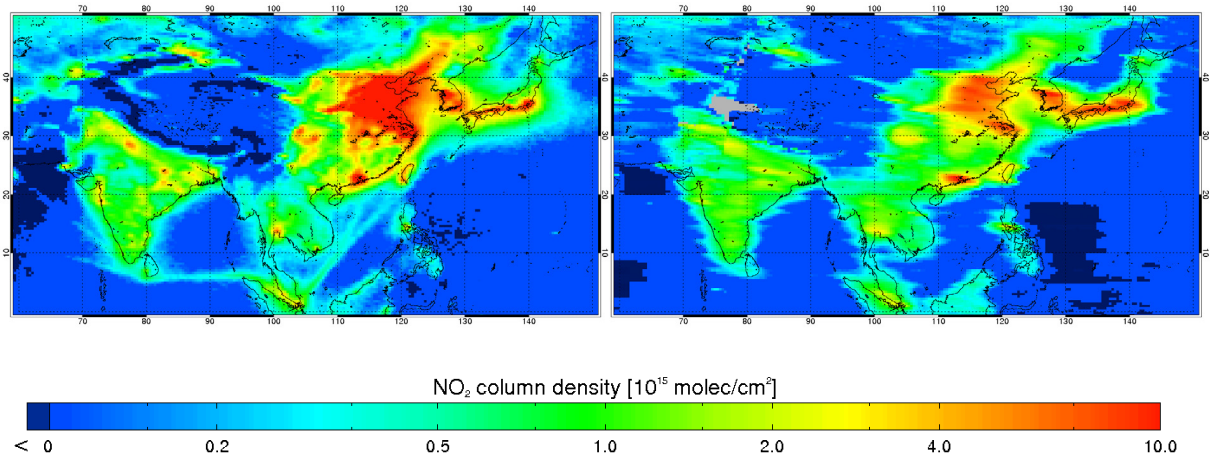

Fig. 4. Average tropospheric NO_2 columns over East Asia measured by GOME-2 for 2007–2009 (left) and by GOME/ERS-2 for 1997–1999 (right).

the clean tropical Pacific region (20° S–20° N; 160°–180° E). This region is divided into small boxes (2° × 2°), and from the variation of the NO_2 columns within each box, an estimate of the slant column precision can be made. (Note that the variability of the air mass factors within the boxes is small (<0.2 %), and is taken into account by scaling the slant columns with an appropriate geometrical air mass factor). The analysis is based on the assumption that the variation in the total NO_2 columns in each box is a result of errors in the slant column only, originating from (random) instrument measurement noise. The deviation of each GOME-2 measurement from the corresponding box mean value is calculated on a daily basis. The slant column error is then derived from the distribution of the slant column deviations, as shown in Fig. 5 for April 2007. The distribution has a Gaussian shape and from the width of the Gaussian, an average slant column error σ_S of 0.45×10^{15} molec cm^{-2} is estimated for GOME-2 ($\sigma_S \approx 0.42 \times FWHM$). Since the instrument noise is mainly a result of the photoelectron shot noise, the slant column error depends significantly on the cloud fraction and surface albedo. For example, the average slant column error for GOME-2 measurements with cloud fraction <50 % is 0.56×10^{15} molec cm^{-2}, while for measurements with cloud fraction >50 % the average slant column error is 0.38×10^{15} molec cm^{-2}.

The GOME-2 slant column error is larger than the 0.35×10^{15} molec cm^{-2} derived for GOME/ERS-2 using the same method. This is consistent with the higher signal-to-noise ratio and larger ground pixel size of the GOME/ERS-2 measurements. Boersma et al. (2007) report a slant column error of 0.67×10^{15} molec cm^{-2} for the OMI NO_2 measurements, consistent with the smaller signal-to-noise ratio of the OMI instrument which has better spatial resolution.

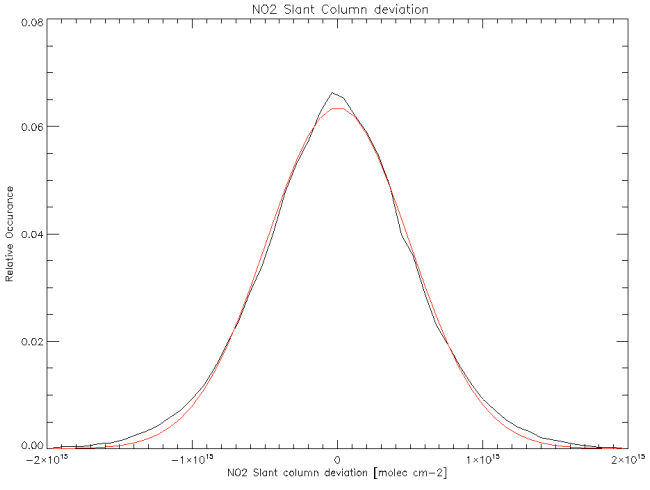

Fig. 5. Distribution of the deviations of GOME-2 NO_2 slant columns from corresponding (2° × 2°) box mean values in the tropical Pacific region (20° S–20° N; 160°–180° E) for April 2007. The red line shows the Gaussian function fitted to the measured distribution. The width of the Gaussian corresponds to a slant column error of 0.45×10^{15} molec cm^{-2}.

The instrument degradation of the GOME-2 sensor in the visible wavelength range of Channel 3 (Lang et al., 2009; Dikty et al., 2010) has an impact on the derived slant column errors, as shown in Fig. 6. In the four years from the start of the operational GOME-2 measurements in January 2007, the GOME-2 slant column error for NO_2 has increase by about 35 %. Here, it should be noted that during the more than 10 yr of GOME/ERS-2 operations, no significant degradation has been detected for the visible wavelength region in Channel 3 (Coldewey-Egbers et al., 2008), and therefore the estimated slant column error for the GOME NO_2 measurements remains relatively constant ($\sim 0.35 \times 10^{15}$ molec cm^{-2}).

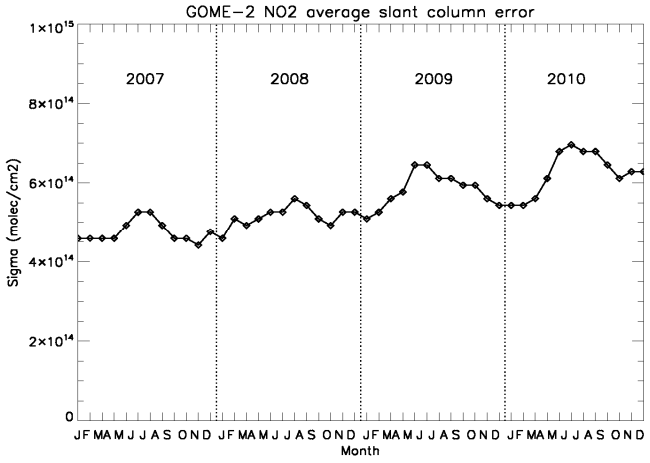

Fig. 6. Estimated NO_2 slant column error for the GOME-2 instrument for the period January 2007–December 2010.

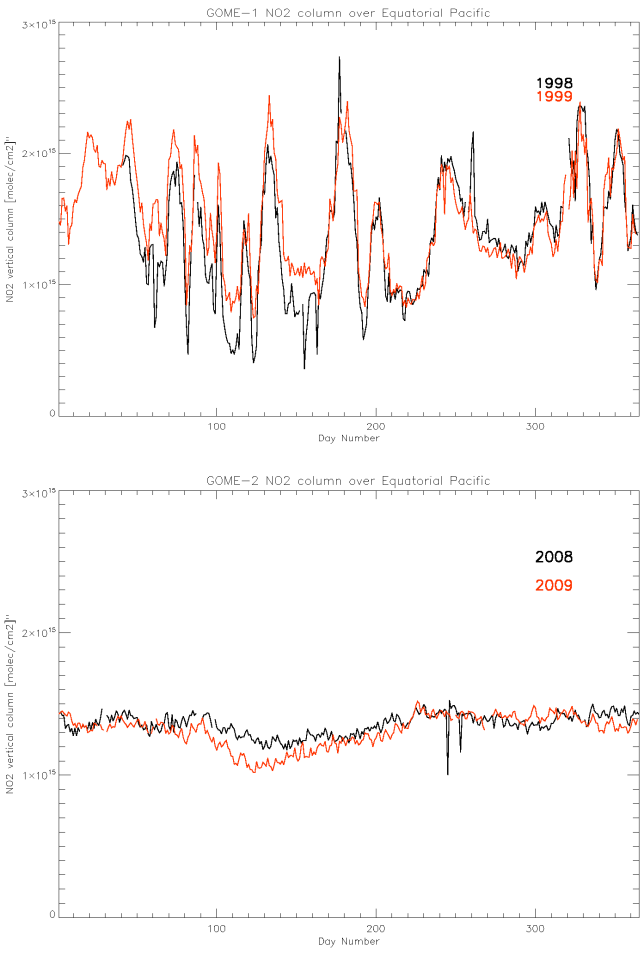

Fig. 7. NO_2 vertical column density from GOME/ERS-2 for the Equatorial Pacific for 1998 and 1999 (top), and from GOME-2/MetOp for 2008 and 2009 (bottom). The GOME NO_2 columns show large and systematic seasonal variations induced by the diffuser plate. The seasonal structures in the GOME-2 NO_2 columns are much smaller as a result of the use of a quartz quasi-volume Diffuser in the GOME-2 instrument.

The spectral structures in the BSDF of the ground aluminium diffuser plate used for the direct sun measurements with GOME/ERS-2 result in spectral features in the differential spectra that correlate with the NO_2 absorption features (Richter and Wagner, 2001; Wenig et al., 2004). This severely affects the DOAS retrieval, resulting in a systematic error of up to 100 % in the GOME NO_2 columns in the tropics. This error appears as temporal variations in the NO_2 time-series with a seasonal component related to the annual cycle in the elevation and azimuth angles of the incoming solar radiation (see Fig. 7 (top)). The quartz quasi-volume diffuser used in the GOME-2 instrument has strongly reduced differential structures in the BSDF and therefore, the induced spectral features in the GOME-2 solar spectra are much smaller. This is clearly visible in the NO_2 time-series for the tropics, as shown in Fig. 7 (bottom). The seasonal patterns in the NO_2 time-series from GOME-2 are more than five times smaller than for GOME/ERS-2 (see also Richter et al., 2011).

Another source of systematic error in the NO_2 slant column is the uncertainty in the laboratory absorption cross-section of NO_2. As described in Sect. 3, the GDP 4.4 algorithm uses the GOME-2 FM cross-sections. Comparisons of the GOME-2 FM cross-sections with the Vandaele et al. (1998) NO_2 cross-sections at 294 K (convolved with the GOME-2 slit function) show a good agreement, with a mean deviation of ∼2 % (Gür et al., 2005; De Smedt, personal communication, 2009). This is consistent with earlier comparisons between various laboratory measurements of NO_2 cross section spectra by Vandaele et al. (1998), which showed mutual agreement of 2 % as well. As discussed in Sects. 3 and 4, the temperature dependence of the NO_2 cross-sections is a potential source of systematic error in the NO_2 slant columns, and an a-posteriori correction for the difference between the atmospheric temperature and the cross-section temperature used in the DOAS-fit (243 K) is applied in the GDP 4.4 algorithm. Neglecting the atmospheric temperature variations and assuming a fixed NO_2 temperature of 243 K would result in large systematic errors up to 20 % (Boersma et al., 2004; Nüß et al., 2006). Assuming a difference between model and real atmospheric temperature of 5 K at the altitude of NO_2 absorption, an additional uncertainty of 2 % in the tropospheric NO_2 columns results.

6.2 Uncertainties in the stratospheric air mass factor and stratospheric column

The stratospheric air mass factor, as used for the initial total VCD calculation, depends mainly on the viewing geometry. The variation in the stratospheric air mass factor due to the NO_2 profile shape, the albedo and cloud cover is ∼2–3 %

for solar zenith angles smaller than ∼80°. For higher solar zenith angles, the variation increases up to 5 %. In the GDP 4.4, the dependence on the stratospheric NO_2 profile shape, the albedo and cloud cover is taken into account in the calculation of the stratospheric air mass factor (see Sect. 4). A conservative estimate of the uncertainty in the stratospheric air mass factor of 2 % is assumed in this study.

In Boersma et al. (2004), the uncertainty in the stratospheric column calculation for GOME/ERS-2 has been estimated for various separation methods. For the reference sector and spatial filtering methods, they found uncertainties of 0.2–0.45 $\times 10^{15}$ molec cm^{-2}. To analyse the uncertainty in the GOME-2 stratospheric column, the spatial filtering method used in the GDP 4.4 has been applied to one year (2004) of reanalyses model data from the IFS-MOZART assimilation system (Flemming et al., 2009) as provided by the Monitoring Atmospheric Composition and Climate (MACC) project (Hollingsworth et al., 2008). To that end, synthetic slant columns for the locations of all GOME-2 measurements were derived from vertical columns given by the IFS-MOZART model on a 1.125° × 1.125° latitude-longitude grid and processed with the GDP 4.4 algorithm. The differences between the retrieved and original stratospheric columns were then analysed to estimate the uncertainty in the GOME-2 stratospheric columns. Figure 8 shows an example of the stratospheric NO_2 field for 15 March, as derived with the GDP 4.4 using the synthetic slant columns, and the stratospheric NO_2 fields from the IFS-MOZART model for the same day. This figure shows a general good agreement between the GDP 4.4 and IFS-MOZART stratospheric columns with a typical stratospheric NO_2 distribution for March, i.e. relatively low stratospheric columns in the tropics (∼1.5 $\times 10^{15}$ molec cm^{-2}), and higher columns at mid- and high-latitudes (2–3 $\times 10^{15}$ molec cm^{-2}). The stratospheric columns retrieved with the GDP 4.4 also show most of the broad longitudinal variations visible in the IFS-MOZART model, for example in the tropical region with a minimum in the stratospheric columns over the Pacific (∼1.3 $\times 10^{15}$ molec cm^{-2}), and between 30–45° N with local enhancements over the Euro-Asia continent. However, the small-scale variations visible in the IFS-MOZART stratospheric NO_2 field cannot be captured with the GDP 4.4, which is an inherent limitation of the spatial filtering approach.

The uncertainty in the GOME-2 stratospheric NO_2 column has been estimated by calculating the mean absolute difference between the stratospheric columns retrieved with the GDP 4.4 and the original stratospheric columns from the IFS-MOZART model (using one year of model data). The derived uncertainties show a clear seasonal and regional dependency. For the northern mid-latitudes (20–60° N), the monthly averaged uncertainty varies between ∼0.2 $\times 10^{15}$ molec cm^{-2} in summer and 0.3 $\times 10^{15}$ molec cm^{-2} in winter. If only the polluted regions of the northern mid-latitudes are taken into account, the uncertainty increases slightly by about 0.05 $\times 10^{15}$ molec cm^{-2}. For the low-latitudes and southern hemisphere, the estimated uncertainty in the stratospheric column is smaller (∼0.15 $\times 10^{15}$ molec cm^{-2}). These values are consistent with previous estimates for GOME/ERS-2 as described above, and with estimates for the OMI NO_2 product (∼0.2 $\times 10^{15}$ molec cm^{-2}, see Bucsela et al., 2006).

Note that for individual days, the uncertainty in the stratospheric NO_2 column can be larger than the monthly averaged values described above, especially in winter near the polar vortex, as shown in Fig. 1 for 22 February 2008. Figure 9 shows the stratospheric NO_2 field from the IFS-MOZART model for this day, and the one derived with the GDP 4.4 using the synthetic slant columns. Comparing the stratospheric NO_2 field from the IFS-MOZART model (Fig. 9 (left)) with the initial GOME-2 total NO_2 columns for this day (Fig. 1 (left)) indicates that the IFS-MOZART model provides an accurate representation of the variation in the stratospheric field on this day. However, as can be seen in Fig. 9 the GDP 4.4 overestimates the stratospheric NO_2 column over Western Europe by ∼0.5 $\times 10^{15}$ molec cm^{-2}. The main problem for the spatial filtering and masking approach in this case is the large gradient in the stratospheric column over a polluted region (Western Europe), which is masked-out before the spatial filtering.

6.3 Uncertainty in the tropospheric air mass factor

As described in Sect. 5.2, the tropospheric air mass factor depends mainly on the surface albedo, the cloud fraction and cloud-top pressure, as well as the a priori NO_2 profile shape. The uncertainty in the air mass factor due to the uncertainty in the surface albedo and cloud parameters was estimated in a sensitivity study on one year (2008) of GOME-2 data, by linearizing the air mass factor and varying the value for these foreward model parameters around the optimal value used in the retrieval.

The uncertainty for the TOMS/GOME surface albedo used in the GDP 4.4 algorithm is assumed to be 0.02 (Boersma et al., 2004). This estimate is in agreement with recent comparisons between TOMS, GOME and OMI LER data, and MODIS black sky albedo, which show average differences smaller than 0.02 between the various surface albedo datasets (Kleinpool et al., 2008). Using this value in the sensitivity study on one year of GOME-2 data, the average uncertainty in the air mass factor due to the surface albedo uncertainty was found to be ∼14 % for polluted conditions with maximum values of up to 30 %. For clean and moderately polluted conditions, the derived uncertainty in the air mass factor is smaller (∼6 %).

The uncertainty in the air mass factor due to the uncertainty in the cloud fraction and cloud-top pressure has been estimated using GOME-2 measurements with cloud radiance fraction <50 % only. For small cloud fractions, the estimated uncertainty in the OCRA cloud fraction is ∼0.06 (Loyola et

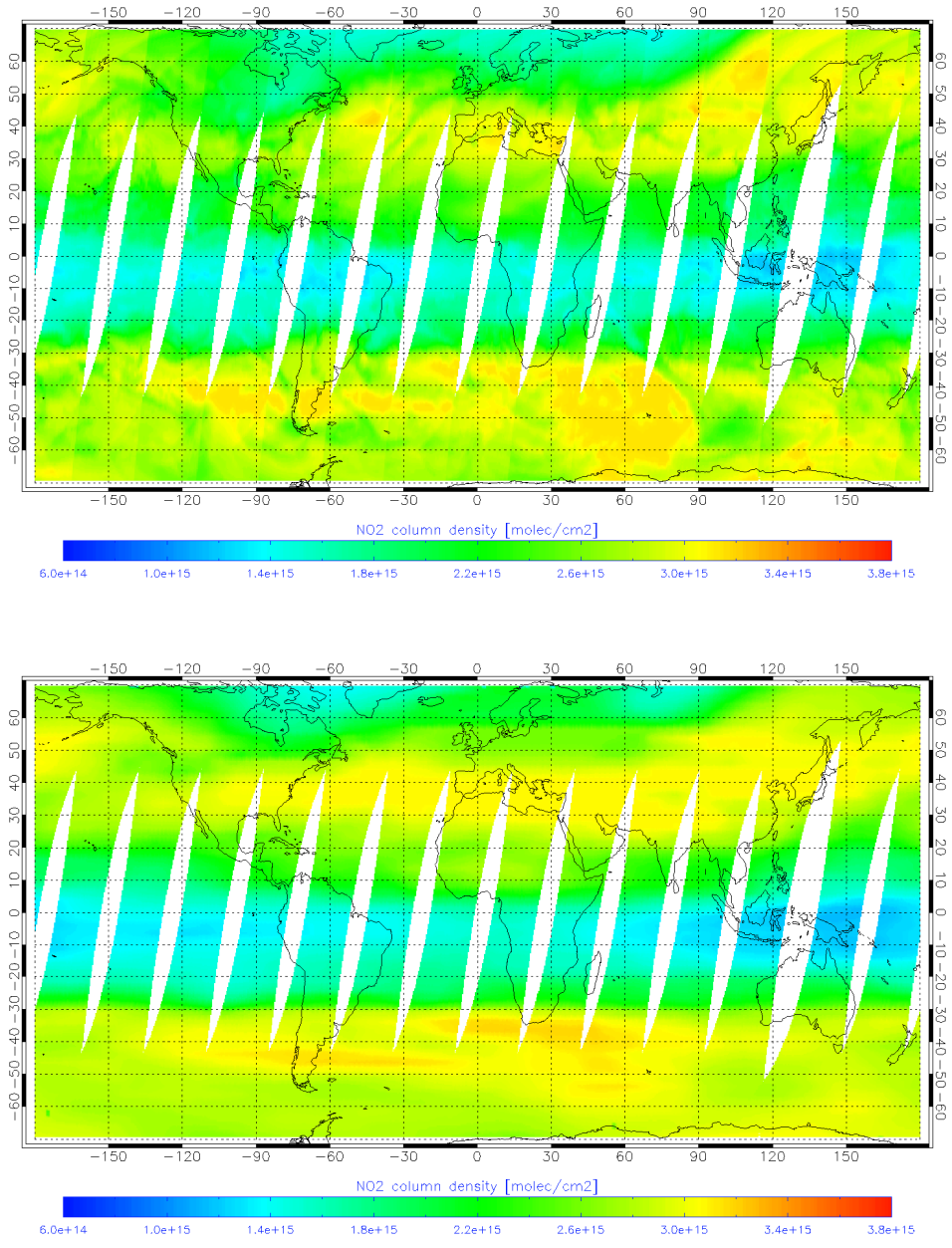

Fig. 8. Stratospheric NO_2 columns from the IFS-MOZART reanalysis model for 15 March 2004 (Top) and those retrieved with the spatial filtering method (as used in the GDP 4.4), using synthetic slant column derived from IFS-MOZART model data as input (Bottom).

al., 2007). The effect of this uncertainty on the tropospheric columns depends mainly on the tropospheric NO_2 load, the surface albedo and cloud-top pressure. The effect of uncertainties in the cloud-top pressure is largest at altitudes with the largest NO_2 concentrations, which is usually within the boundary layer. For clouds in the lower troposphere (cloud top pressure >700 hPa), the uncertainty in the ROCINN cloud-top pressures is $\sim$40 hPa (Loyola et al., 2011).

From the sensitivity study on one year of GOME-2 data, the derived uncertainty in the tropospheric air mass factor due to the cloud fraction uncertainty is in the 5–50 % range, with an average uncertainty of $\sim$25 % for polluted regions. Figure 10 shows the average error in the tropospheric air mass factor for March 2008 due to uncertainty in the GOME-2 cloud fraction. The effect of the cloud fraction uncertainty is largest for areas with enhanced tropospheric NO_2 at low altitudes and small surface albedo, such as the continental source regions. Also clearly visible in Fig. 10 are the ship tracks and the coastal areas with relative large NO_2

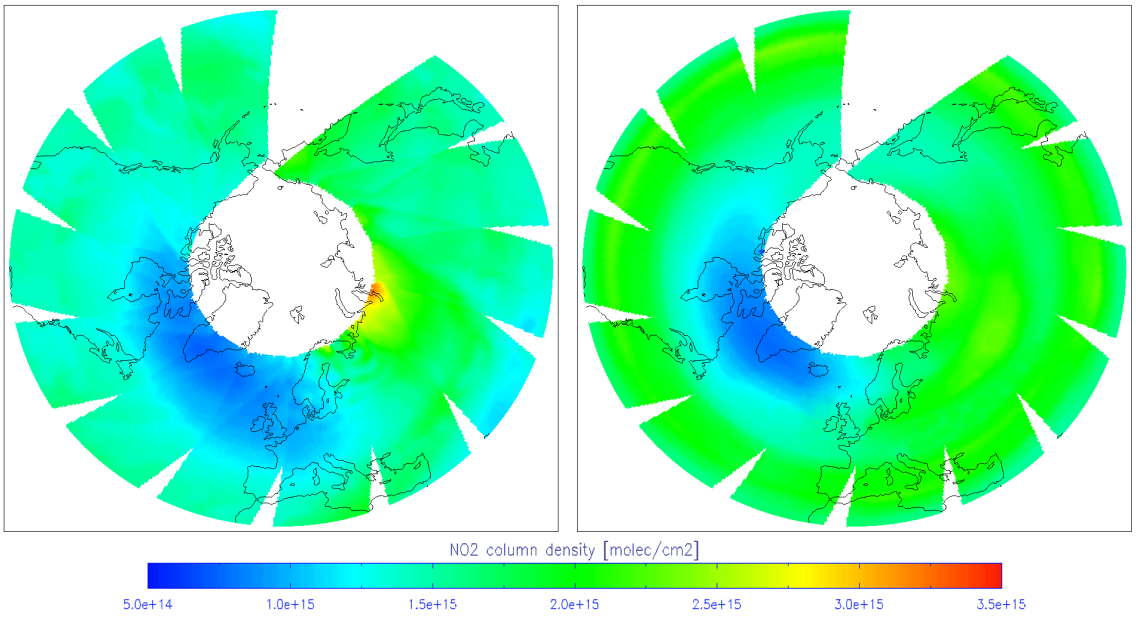

Fig. 9. Stratospheric NO_2 columns from the IFS-MOZART reanalysis model for 22 February 2008 (left) and those retrieved with the spatial filtering method (as used in the GDP 4.4), using synthetic slant column derived from IFS-MOZART model data as input (right).

concentrations in the boundary layer compared to the cleaner oceans. Since the ROCINN cloud-top pressures are usually above the NO_2 pollution layer, the average uncertainty in the tropospheric air mass factor due to the cloud top pressure uncertainty is relatively small (∼3 %). Note that for individual GOME-2 measurements, the uncertainty can be ∼30 % or larger, when the cloud is located inside the NO_2 pollution layer.

The NO_2 profile shape assumed for the airmass factor calculation also has a large effect on the airmass factor, in particular over dark surfaces where the measurement sensitivity decreases towards the surface. Boersma et al. (2004) evaluated this uncertainty by analysing the variability in the NO_2 profiles from the TM3 chemistry-transport model that they used as a priori, and estimated an uncertainty of 10 % on average but much larger values locally. In the GDP 4.4, monthly averages of MOZART profiles for one year (1997) are applied which introduces additional uncertainties as the effects of day-to-day variations in meteorology are not included. In order to quantify this source of uncertainty, daily and monthly airmass factors were calculated for two months of MOZART model data (January and July) (Nüß et al., 2006). The relative RMS of the daily values was between 5 % and 10 % for most locations with maxima of up to 20 %. From this result, the uncertainty introduced by the use of monthly airmass factors is estimated to be 10 %. The larger value was selected to account for the possibility of additional inter-annual changes, e.g. from changes in NO_x emission strengths or transport patterns.

Table 2. Estimated mean uncertainty in the tropospheric air mass factor M_t for polluted conditions ($V_t > 1.0 \times 10^{15}$ molec cm^{-2}) due to errors in the surface albedo, cloud parameters, and the a priori NO_2 profile shape.

Error source	Uncertainty	Uncertainty in M_t
Surface albedo	0.02	14 %
Cloud fraction	0.06	25 %
Cloud–top pressure[1]	40 hPa	3 %
NO_2 profile shape	see Sect. 6.3	15 %
Total uncertainty[2]		33 %

[1] The uncertainty in M_t due to the error in the cloud-top pressure is highly variable, see Sect. 6.3. [2] The uncertainty due to the effect of aerosols is not included, see Sect. 6.3.

Table 2 summarizes the estimated uncertainties in the tropospheric air mass factor for polluted conditions ($V_t > 1.0 \times 10^{15}$ molec cm^{-2}). The total uncertainty in the tropospheric air mass factor is mostly in the 15–50 % range, with an average uncertainty of ∼33 %. The total uncertainty in the tropospheric NO_2 column can be estimated with Eq. (8), and range from 40 to 80 % for polluted conditions (see Table 3).

Aerosols are not included in the radiative transfer calculations performed in the GDP 4.4 retrieval. This is similar to the situation in most other retrievals (e.g. Bucsela et al., 2006; Boersma et al., 2007) and introduces uncertainties in the calculations of airmass factors and cloud properties. Leitão et al. (2010) have investigated the effect of aerosols

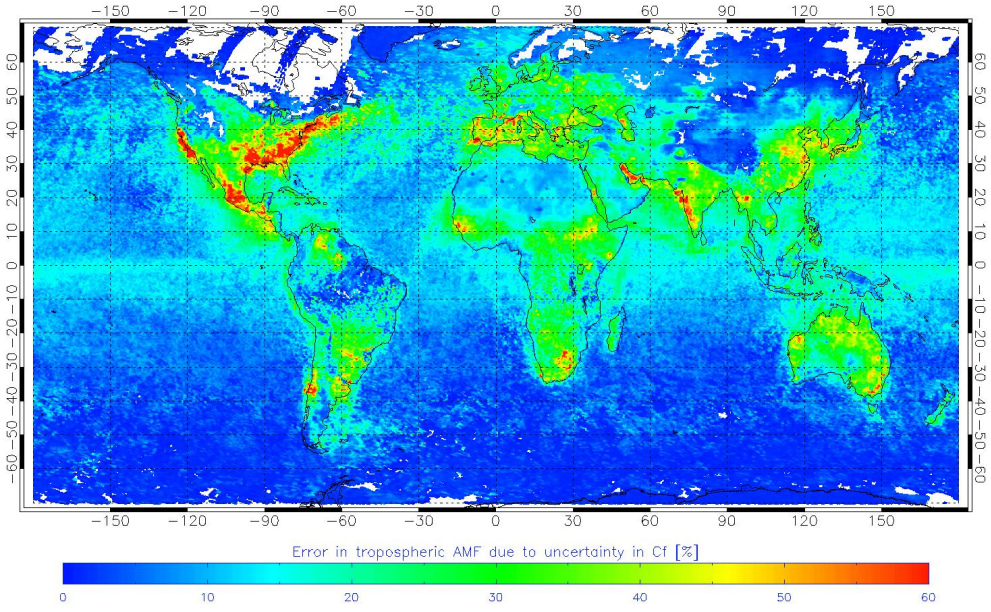

Fig. 10. Uncertainty in the tropospheric air mass factor for March 2008 due to the uncertainty in the GOME-2 cloud fraction. Only measurements with a cloud radiance fraction <50 % were used.

on airmass factors in clear-sky scenarios for both idealised and more realistic scenarios. They found largely varying effects ranging from just a few percent up to a factor of 2 of reductions and enhancements of the airmass factors depending on AOD, single scattering albedo and relative vertical position of NO_2 and aerosol. However, the cloud treatment will provide some implicit correction of the aerosol effects as discussed in Boersma et al. (2004). In fact, in a recent study, Boersma et al. (2011) show that in very clear situations over the Eastern US, the OMI cloud fraction is well correlated to aerosol optical thickness retrieved from MODIS and that the implicit correction of the airmass factor is similar to that derived from an explicit radiative transfer calculation. However, it is not clear if this finding also holds for partly cloudy scenes and other regions of the world. A full treatment of aerosols in the radiative transfer will only be possible if clouds and aerosols are represented as scattering layers (as e.g. in Martin et al., 2002) and if detailed information on aerosol optical properties is available.

7 Ground-based validation methodology

Ground-based Multi-Axis MAXDOAS instruments operated at many stations around the world provide tropospheric and stratospheric NO_2 columns using retrievals similar to those applied to satellite data. However, significant differences in sensitivity between satellite and ground-based NO_2 measurement systems exist and should be carefully taken into account when dealing with the validation of NO_2 columns derived from GOME-2. Atmospheric NO_2 exhibits large natural structures and cycles, among which are a vertical profile and a geographical distribution varying drastically with latitude and with the presence of emissions, and a diurnal cycle of photochemical origin. Differences in sampling and smoothing of these structures and cycles can hamper the comparison of GOME-2 and correlative observations if not taken into account properly. While the validation of stratospheric NO_2 columns derived from satellite can count on past experience based on an extended ground-based network of zenith sky light (ZSL) DOAS instruments covering different ranges of NO_2 values as part of the Network for the Detection of Atmospheric Composition Change (NDACC, Kurylo and Zander, 2000), the validation of tropospheric NO_2 data is still a matter of research. The development of appropriate instruments and validation methodologies remains an objective for field intercomparison campaigns, like the DANDELIONS and the CINDI campaigns (Brinksma et al., 2008; Roscoe et al., 2010).

Table 3. Contributions to the overall uncertainty in the GOME-2 tropospheric NO_2 column retrieved with the GDP 4.4 for polluted conditions ($V_t > 1.0 \times 10^{15}$ molec cm^{-2}).

Error source	Uncertainty
Slant column	0.45×10^{15} molec cm^{-2}
Stratospheric column	$0.15–0.30 \times 10^{15}$ molec cm^{-2}
Tropospheric AMF	15–50 %
Tropospheric column	40–80 %

As mentioned in Sect. 5, the retrieval of tropospheric NO_2 from satellite measurements is a complex process based on a chain of individual retrieval modules, each one relying on a set of assumptions. For this reason, a reliable validation of the final product should assign a validity indicator to each critical individual component of the level-1-to-2 retrieval chain. As a consequence, the validation of GOME-2 NO_2 columns in the O3M-SAF context has been set up as an end-to-end approach (Lambert et al., 2008), consisting in the validation of each component of the retrieval, as recommended by Reference Protocols and Guidelines (CEOS 2004, Lambert et al., 2009). This approach is essential in that it allows hidden compensating errors to be unravelled. The end-to-end validation approach adopted for GOME-2 NO_2 data successively addresses the validity of: (a) DOAS analysis results, (b) the stratospheric reference and (c) tropospheric NO_2 column data. An illustration of such a three level validation strategy is presented hereafter, based on measurement results obtained at the Observatoire de Haute Provence (OHP, 44° N, 5.7° E) station from March 2007 to March 2011. In a forthcoming paper, this kind of exercise will be extended including more ground-based measurements, covering different pollution levels.

Although not exploited in the present study, MAXDOAS instruments can provide vertically resolved information on both tropospheric NO_2 and aerosols in the lower troposphere. This may be used to the benefit of advanced validation studies where the sensitivity of satellite AMFs to uncertainties on the a-priori information on NO_2 profile shape and aerosol could be investigated.

8 End-to-end GOME-2 NO_2 validation at the OHP station

To illustrate the end-to-end validation of the operational GOME-2 NO_2 data product as retrieved with the GDP 4.4, a complete set of correlative observations available at the OHP station is used. Slant, total, stratospheric and tropospheric columns are separately assessed as to their "validity" in comparison to ground-based MAXDOAS observations as well as other satellite datasets, such as the operational NO_2 product from GOME/ERS-2 (Lambert and Balis, 2004) and the TEMIS NO_2 products from SCIAMACHY (Blond et al., 2007; Boersma et al., 2004).

8.1 Ground-based MAXDOAS observations

The Belgian Institute for Space Aeronomy (BIRA-IASB) has been operating a MAXDOAS instrument at the NDACC station OHP since 2005 and in the framework of the O3M-SAF, these data have been used to test and set up a method for the validation of the operational GOME-2 NO_2 product (Lambert et al., 2008). Although it is largely rural, OHP can occasionally be influenced by polluted air masses transported from neighbouring cities, hence providing interesting test cases for GOME-2 sensitivity to tropospheric NO_2. The MAXDOAS technique has been developed as an extension of the ZSL-DOAS technique, for the determination of vertically resolved abundances of atmospheric trace species in the lowermost troposphere (Hönninger et al., 2004; Wagner et al., 2004; Wittrock et al., 2004; Heckel et al., 2005). MAXDOAS instruments collect scattered sky light in a series of line-of-sight (LOS) angular directions extending from the horizon to the zenith. High sensitivity towards absorbers present near the surface is obtained for the smallest elevation angles, while measurements at higher elevation provide information on the rest of the column. In this way, a separation between near-surface concentration, tropospheric column and stratospheric column can be obtained. The MAXDOAS instrument at OHP is based on a grating spectrometer covering the 330–390 nm range and NO_2 differential slant column densities (DSCDs) are retrieved in the 364–384 nm wavelength interval range using the DOAS technique. More information on the instrument and the retrieval settings can be found in Lambert et al. (2008) and Pinardi et al. (2008).

8.2 Slant columns

Figure 11 shows time series and scatter plot of monthly averaged normalized slant columns measured from January 2007 until July 2010 within 300 km around OHP by different satellites: GOME (GDP 4.1), SCIAMACHY (TEMIS v1.10) and GOME-2 (GDP 4.4). The slant columns have been normalised by their geometrical air mass factor in order to consider the different angular dependencies of the three satellite instruments resulting from differences in the local overpass time and scanning angles. Error bars represent the variability (one sigma standard deviation) in the measurements. Note the significant increase of the standard deviations for all instruments during the winter periods, which can be explained by a larger contribution from tropospheric pollution events and by the larger variability in the stratospheric NO_2 column in winter.

Considering the combined variability in the slant column data and the remaining instrumental differences (such as the different degradation of the three instruments and the effect of the diffuser plate anomaly which introduces time-dependent pseudo-random variations in the measured columns, especially for GOME/ERS-2), one can conclude that all satellite data sets agree within their uncertainties.

8.3 Total and stratospheric columns

Figure 12 shows the initial total VCD (i.e. computed with stratospheric air mass factors, and thus "uncorrected" for tropospheric pollution) of GOME-2, and the corresponding stratospheric column V_s above OHP, for different cloud selections. All GOME-2 measurements within 300 km of OHP between March 2007 and July 2010 are selected and binned

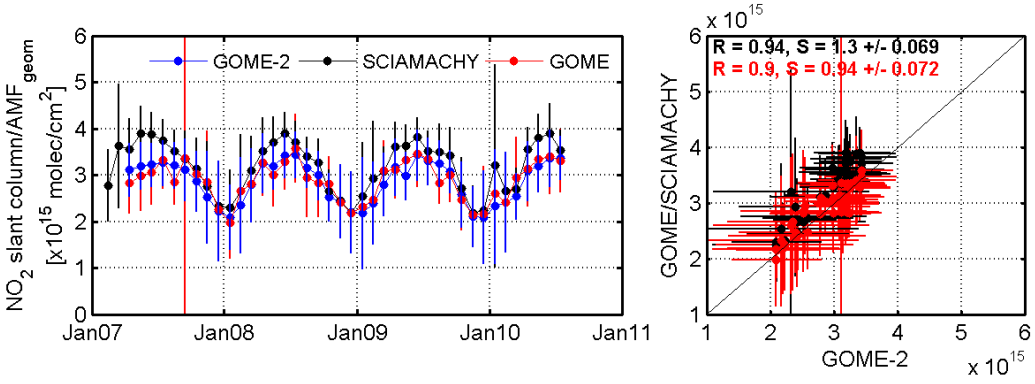

Fig. 11. Comparison of normalized NO_2 slant column densities as measured by GOME (GDP 4.1), SCIAMACHY (TEMIS v1.10) and GOME-2 (GDP 4.4) at the Observatoire de Haute Provence (OHP, 44° N, 5.7° E) between January 2007 and July 2010. Dots represent the monthly average of all satellite measurements within a radius of 300 km around OHP and the error bars the one sigma variability. The left panel shows the time series of the three datasets, while the right panel presents the scatter plot of the GOME and SCIAMACHY datasets with respect to the GOME-2 data. The correlation coefficient R and the slope S of the orthogonal regression line are given as insert.

according to cloud fractions. The left panel corresponds to a selection of high clouds (cloud top pressure (CTP) smaller than 400 hPa) while the right panel corresponds to lower clouds (CTP larger than 400 hPa). As expected, the stratospheric content is similar in both plots, while the total (uncorrected) VCD strongly depends on the bulk altitude of the clouds. High clouds effectively mask the signal from surface NO_2 while in case of low-lying clouds, the satellite observations are sensitive to a part of the tropospheric NO_2 column, even for fully cloudy pixels, and the sensitivity is further increased for NO_2 above the cloud.

For the validation of satellite NO_2 columns, twilight sunrise zenith sky light (ZSL) data from SAOZ and DOAS-like instruments, mostly sensitive to stratospheric NO_2, have been used in past studies (Lambert et al., 2004; Ionov et al., 2008; Celarier et al., 2008). Stratospheric NO_2 columns presented here are derived from zenith-sky measurements performed at sunrise between 87°–91° SZA by the BIRA MAXDOAS instrument at OHP. Zenith-sky AMFs are accurately determined using a-priori climatological stratospheric NO_2 profiles (Lambert et al., 2000) similar to those used in the satellite evaluations. GOME-2 data are selected at the intersection with ZSL-DOAS air masses, according to the procedure described in Balis et al. (2007). This approach allows the reduction of horizontal smoothing uncertainties by matching the optical air masses extensions. NO_2 cross-sections used for retrieving the columns are at same temperature (243 K) as used for the satellite data.

Figure 13 shows the comparison between time-series of NO_2 stratospheric column data from GOME-2 (GDP 4.4), SCIAMACHY (TEMIS) and coincident ground-based ZSL measurements performed at OHP between March 2007 and July 2010. The GOME-2 stratospheric columns as derived with the GDP 4.4 are found to be in good overall agreement with the other datasets showing a good correlation and a similar seasonal variation. The mean differences are less than 1.9×10^{14} molec cm^{-2} and less than 8.9×10^{13} molec cm^{-2} respectively compared to the ground-based data and to the SCIAMACHY dataset. The difference between the two satellites datasets is mainly related to the different approach used to infer the stratospheric correction (spatial filtering versus assimilation) and is coherent with the estimated uncertainty for the stratospheric columns in Sect. 6.2. These results are in line with those reported in a previous study using the SAOZ network as a source of correlative data (Ionov et al., 2008).

8.4 Tropospheric columns

The GOME-2 tropospheric NO_2 column has been compared to ground-based MAXDOAS measurements performed at OHP. Here, tropospheric vertical columns are obtained from MAXDOAS differential SCD measurements considering a geometrical approximation for the tropospheric AMF, as described e.g. in Brinksma et al. (2008), Pinardi et al. (2008), and Lambert et al. (2008). Figure 14 shows a time-series of the ground-based MAXDOAS and the GOME-2 tropospheric NO_2 columns over OHP from June 2007 to March 2011. Comparison datasets are selected by taking the daily mean value of all GOME-2 measurements with cloud radiance fraction less than 50 % within 100 km around OHP, and by interpolating the ground-based data at the satellite overpass time. Alternatively ground-based data can be averaged within a prescribed time window around the satellite overpass time, and compared to the spatially closest satellite pixel. Both comparison approaches are found to give similar results with no significant statistical differences (Lambert et al., 2008).

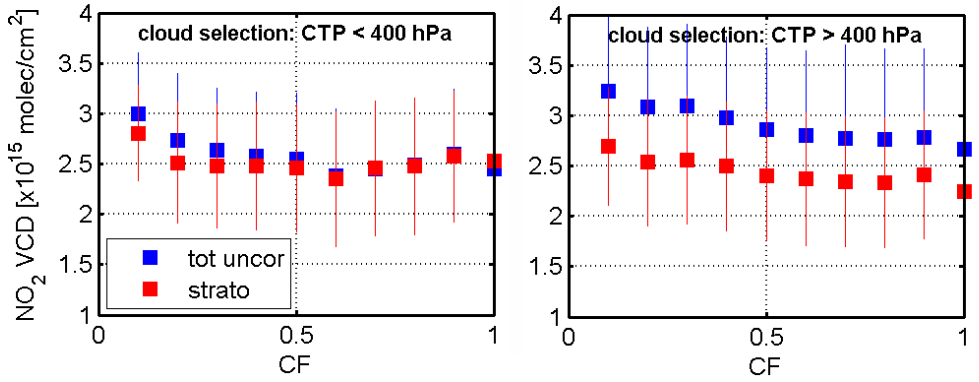

Fig. 12. Comparison of initial total NO_2 columns (i.e. uncorrected for tropospheric pollution) and stratospheric NO_2 columns from GOME-2 around OHP. The squares correspond to NO_2 column averages in bins of 0.1 cloud fraction unit and the error bars to the variability of all pixels in time and space. On the left hand side, GOME-2 measurements with a cloud top pressure (CTP) smaller that 400 hPa are selected, while on the right hand side the selection applies to measurements with a CTP higher than 400 hPa.

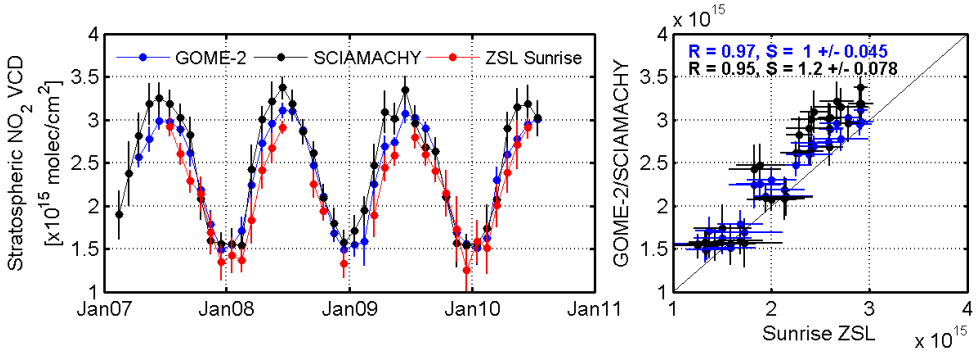

Fig. 13. Comparison of stratospheric NO_2 column data measured by GOME-2 (GDP 4.4), SCIAMACHY (TEMIS v1.10) and ground-based ZSL sunrise measurements from the MAXDOAS instrument at OHP, between January 2007 and July 2010. Left panel: time series of NO_2 monthly means around OHP; right panel: scatter plot between the satellite and the ground-based ZSL measurements. The coefficient R and the slope S of the orthogonal regression line are given as insert.

One can see in Fig. 14 that pollution episodes are well captured by GOME-2, although the scatter of the individual comparison points is relatively large. These results are qualitatively similar to those obtained in previous validation exercises (e.g. Brinksma et al., 2008; Celarier et al., 2008; Irie et al., 2008). However, in our study a much longer comparison dataset is available (∼4 yr) and averaging can be performed, in order to limit the influence of temporal and spatial sensitivity differences on the comparison. As can be seen, monthly mean values are in very good agreement, the seasonal variations in tropospheric NO_2 column being similarly captured by both observation systems. The differences are generally within 0.5×10^{15} molec cm^{-2}, with maximum differences around 2×10^{15} molec cm^{-2}, as for December 2008. During the latter period, however, the comparison was hampered by a lack of ground-based measurement points due to an instrumental deficiency. A scatter plot of the daily and monthly mean values is shown in Fig. 15, as well as the line of a orthogonal regression fit. A correlation coefficient of 0.81, a regression slope of 0.99 ($\pm$0.11) and an intercept of -0.37 ($\pm$0.23) $\times 10^{15}$ molec cm^{-2} are derived when comparing monthly means GOME-2 to the MAXDOAS columns.

The GOME-2 tropospheric columns have also been compared to the SCIAMACHY satellite datasets in Fig. 16. In this case, the monthly means of all satellite "cloud-free" measurements within 100km around OHP are considered. No ground-based data is included in this comparison as for each satellite dataset a different selection of coincident ground-based data would have to be performed. GOME-2 tropospheric NO_2 columns are found to agree well with SCIAMACHY (TEMIS product), considering their combined uncertainties and the large tropospheric NO_2 variability. The temporal variations are similar, and the corresponding scatter plot presents a correlation of 0.78, a regression slope of 0.9 ($\pm$ 0.11) and an intercept of $0.35 \pm (0.24) \times 10^{15}$ molec cm^{-2} .

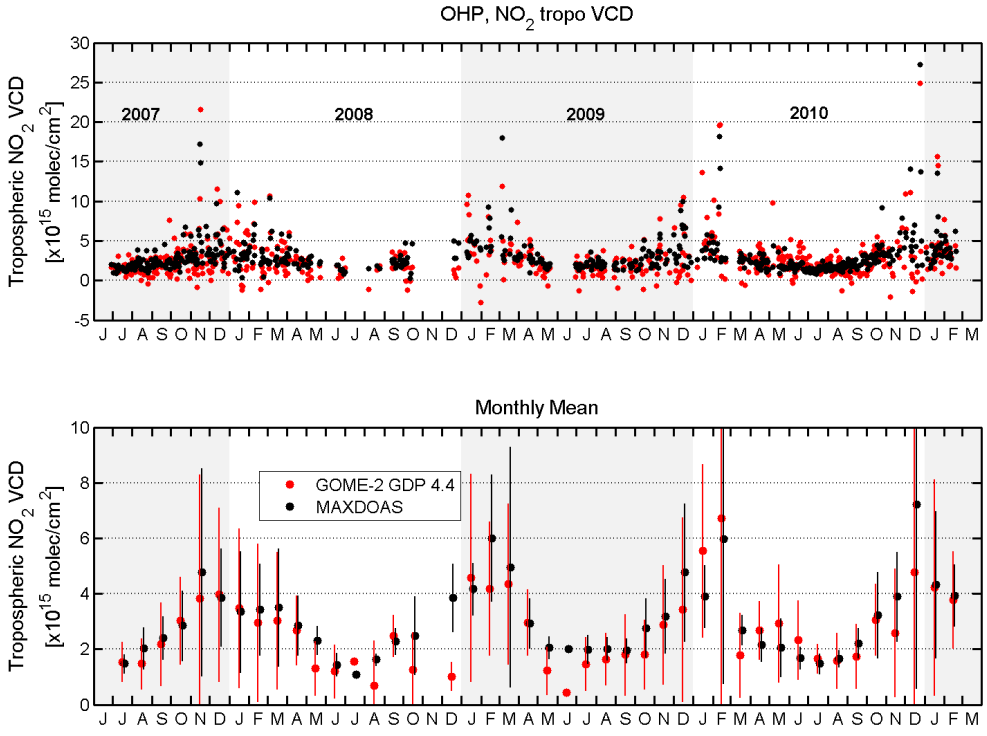

Fig. 14. Comparison of MAXDOAS and GOME-2 tropospheric NO_2 columns (mean value of all the pixels within 100 km around OHP, after cloud-free selection) from June 2007 to March 2011. In the first subplot daily values (only days with both successful measurements) are represented while the second subplot displays monthly averaged values and corresponding one sigma standard deviations (if there was only one coincident MAXDOAS measurement in a particular month, the error bar is omitted).

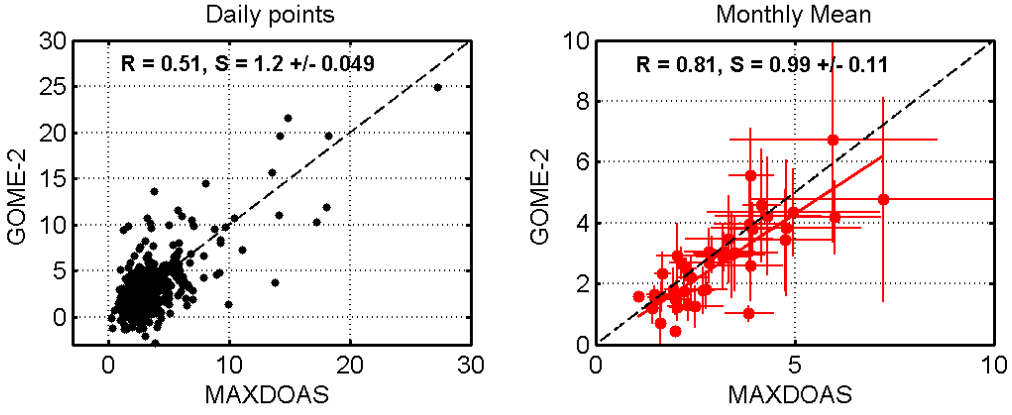

Fig. 15. Scatter plot of the daily (left) and monthly (right) averaged MAXDOAS and GOME-2 tropospheric NO_2 columns at OHP for the period displayed in Fig. 14. The correlation coefficient R and the slope S of the orthogonal regression line are given as insert.

In conclusion, the operational GOME-2 NO_2 column product shows a high level of consistency with correlative observations available at the OHP station. The slant, stratospheric and tropospheric columns derived with the GDP 4.4 agree well with the other datasets. Note that validation results of the operational GOME-2 NO_2 product, addressing both the stratospheric and tropospheric columns are regularly updated within the O3M-SAF, confirming a good global agreement with ground-based correlative data sets (Lambert et al., 2008). More detailed comparisons will be addressed in a forthcoming NO_2 validation paper, including results from the whole NDACC network and more MAXDOAS stations.

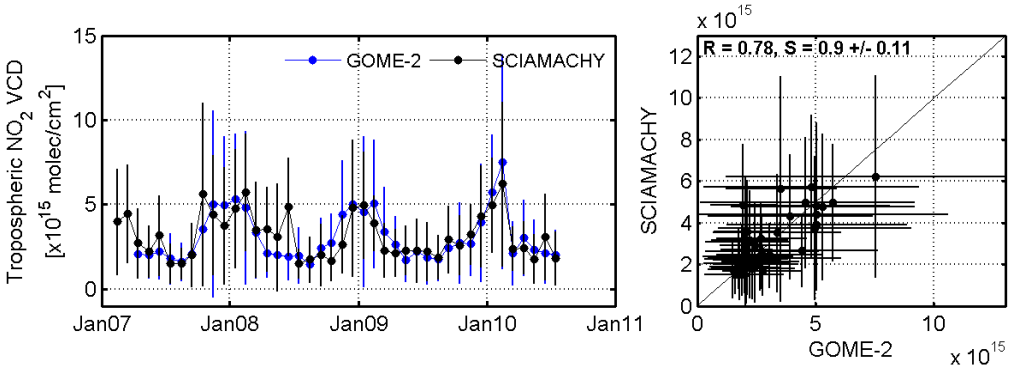

Fig. 16. Comparison of monthly mean tropospheric NO_2 columns measured by GOME-2 (GDP 4.4) and SCIAMACHY (TEMIS v1.10), around OHP between January 2007 and July 2010. Only cloud-free satellite measurements within 100 km of OHP are used for the comparison. The correlation coefficient R and the slope S of the orthogonal regression line are given as insert.

9 Summary and conclusions

In this paper, we have described the operational total and tropospheric NO_2 retrieval algorithms for GOME-2, as implemented in the GOME Data Processor (GDP) version 4.4. The DOAS method is used to determine NO_2 slant column densities from calibrated GOME-2 (ir)radiance data in the 425–450 nm wavelength range. Initial total VCDs are computed using an air mass factor based on a stratospheric NO_2 profile climatology. In the GDP 4.4, a spatial filtering method is used to obtain the stratospheric NO_2 component from the initial total VCD. This method has been shown to be an improvement on the Pacific reference sector method, which rests on the assumption of a longitudinally homogeneous stratospheric NO_2 layer. For the tropospheric air mass factor computation, monthly average NO_2 profiles from the MOZART-2 CTM are used, determined for the satellite overpass time. GOME-2 derived cloud properties, determined with the OCRA and ROCINN algorithms are used to calculate the air mass factors for scenarios in the presence of clouds. Example applications of the GOME-2 tropospheric NO_2 columns show the increased spatial detail compared to its predecessor GOME/ERS-2, which is results of the better spatial coverage and resolution of the GOME-2 instrument.

A statistical approach has been used to estimate the uncertainty in the GOME-2 slant columns. We find that the random error in the slant column is approximately 0.45×10^{15} molec cm^{-2}. In the four years from the start of GOME-2 measurements in 2007, the slant column error has increased by about 35 % due to the instrument degradation of the GOME-2 sensor. As a result of the improved quartz diffuser plate used in the GOME-2 instrument, the systematic error in the slant columns is strongly reduced compared to GOME/ERS-2. The estimated uncertainty in the stratospheric NO_2 column determined with the spatial filtering method is in the $0.15–0.3 \times 10^{15}$ molec cm^{-2} range. The most important uncertainties associated with the computation of the tropospheric air mass factor are cloud fraction, surface albedo and the a priori NO_2 profile. The estimated uncertainty in the tropospheric NO_2 column for polluted conditions ranges from 40 to 80 %.

We have also presented an end-to end ground-based validation approach for the GOME-2 NO_2 product, involving the validation of each component of the retrieval. This end-to-end validation was illustrated for four years (January 2007–March 2011) of GOME-2 NO_2 measurements based on MAX-DOAS measurements at the Observatoire de Haute Provence (OHP; 44° N, 5.7° E). The stratospheric columns from GOME-2 and coincident ground-based measurements at OHP are found to be in good overall agreement. A time series of the MAX-DOAS and the GOME-2 tropospheric NO_2 columns shows that pollution episodes at OHP are well captured by GOME-2. Monthly mean tropospheric columns are in very good agreement, with differences generally within 0.5×10^{15} molec cm^{-2}.

Future versions of the operational NO_2 algorithm for GOME-2 will benefit from recent developments in the NO_2 slant column retrieval as described by Richter et al. (2011). By using an extended DOAS fitting window (425–497 nm) the noise in the GOME-2 slant columns can be significantly reduced. Furthermore, the large scatter of the NO_2 columns in the region affected by the Southern Atlantic Anomaly (SAA) can be reduced by removing the noisy spectral points (spikes) from the DOAS fit and identifying such pixels already in the GOME-2 level-0-to-1 processing. Improvements to the stratospheric correction approach are currently under investigation, with a view on the treatment of background NO_2 column variability in the spatial filtering procedure and on improving the pollution masking using recent MOZART model results. The air mass factor and cloud algorithms can be improved by using the new MERIS black-sky albedo climatology (Popp et al., 2011). MERIS has an equator crossing time (10:30 LT) close to that of GOME-2 and the MERIS albedo data-set has a good spatial resolution of

0.25° latitude × 0.25° longitude. The MERIS albedo climatology at 442 nm can be used for the NO_2 air mass factor calculations, while for the ROCINN cloud retrieval in the O_2 A-band, the MERIS data at 754 nm and 775 nm can be used. The use of an updated a priori NO_2 profile climatology based on global CTM results for 2007–2010 will further improve the tropospheric air mass factor computation. The option to use daily NO_2 profiles from an online CTM that captures the short-term variability in the NO_2 fields is also under consideration for future versions of the GDP. Research on the use of an improved cloud model in the NO_2 retrieval, where clouds are presented as scattering layers is ongoing (Spurr et al., 2009). Similarly, the representation of aerosols as scattering layers will allow full treatment of aerosols in the radiative transfer calculations if detailed information on aerosol optical properties is available.

The GOME-2 total and tropospheric NO_2 products are generated operationally at the O3M-SAF processing facility in DLR, and cover the period from January 2007 onwards. The GDP 4.4 algorithm is shown to be robust in performance and more than capable of real-time data turnover in operational execution. Near-real-time (i.e. two hours after sensing), offline and re-processed products are freely available. The GOME-2 NO_2 products are broadcasted via EUMETCast and WMO/GTS, and are available online on a FTP server. GOME-2 products can also be ordered at the Help Desk of the O3M-SAF hosted by the Finnish Meteorological Institute (FMI) (o3msaf@fmi.fi). The GOME-2 Algorithm Theoretical Basis Document (ATBD), Product User Manual (PUM), Validation Reports, as well as quick-look images and links to related services are available from following DLR web page: http://atmos.caf.dlr.de/gome2.

Acknowledgements. Development of the GOME-2 NO_2 column products and their validation has been funded by the O3M-SAF project with EUMETSAT and national contributions. Part of this work was funded by ProDEx and the Belgian Science Policy via SECPEA. The authors would like to thank F. Boersma (KNMI) for useful discussions. We thank W. Zimmer and L. Butenko for the development work on the UPAS system. S. Kiemle, J. Jaeger, K. H. Seitz, B. Huber and T. Ruppert are kindly acknowledged for the day-to-day operations of the O3M-SAF facility at DLR. We thank EUMETSAT for the ground-segment interfacing work with the O3M-SAF systems and for the provision of GOME-2 level 1 products.

Edited by: T. von Clarmann

References

Antón, M. and Loyola, D.: Influence of cloud properties on satellite total ozone observations, J. Geophys. Res., 116, D03208, doi:10.1029/2010JD014780, 2011.

Balis, D., Lambert, J.-C., Van Roozendael, M., Spurr, R., Loyola, D., Livschitz, Y., Valks, P., Amiridis, V., Gerard, P., Granville, J., and Zehner, C.: Ten years of GOME/ERS2 total ozone data – The new GOME data processor (GDP) version 4: 2. Ground-based validation and comparisons with TOMS V7/V8, J. Geophys. Res., 112, D07307, doi:10.1029/2005JD006376, 2007.

Beirle, S., Platt, U., Wenig, M., and Wagner, T.: Weekly cycle of NO_2 by GOME measurements: a signature of anthropogenic sources, Atmos. Chem. Phys., 3, 2225–2232, doi:10.5194/acp-3-2225-2003, 2003.

Beirle, S., Platt, U., von Glasow, R., Wenig, M., and Wagner, T.: Estimate of nitrogen oxide emissions from shipping by satellite remote sensing, Geophys. Res. Lett., 31, L18102, doi:10.1029/2004GL020312, 2004.

Blond, N., Boersma, K. F., Eskes, H. J., van der A, R. J., Van Roozendael, M., De Smedt, I., Bergametti, G., and Vautard, R.: Intercomparison of SCIAMACHY nitrogen dioxide observations, in-situ measurements and air quality modeling results over Western Europe, J. Geophys. Res, 112, D10311, doi:10.1029/2006JD007277, 2007.

Boersma, K. F., Eskes, H. J., and Brinksma, E. J.: Error analysis for tropospheric NO_2 retrieval from space, J. Geophys. Res., 109, D04311, doi:10.1029/2003JD003962, 2004.

Boersma, K. F., Eskes, H. J., Veefkind, J. P., Brinksma, E. J., van der A, R. J., Sneep, M., van den Oord, G. H. J., Levelt, P. F., Stammes, P., Gleason, J. F., and Bucsela, E. J.: Near-real time retrieval of tropospheric NO_2 from OMI, Atmos. Chem. Phys., 7, 2103–2118, doi:10.5194/acp-7-2103-2007, 2007.

Boersma, K. F., Jacob, D. J., Eskes, H. J., Pinder, R. W., Wang, J., and van der A, R. J.: Intercomparison of SCIAMACHY and OMI tropospheric NO_2 columns: Observing the diurnal evolution of chemistry and emissions from space, J. Geophys. Res., 113, D16S26, doi:10.1029/2007JD008816, 2008.

Boersma, K. F., Eskes, H. J., Dirksen, R. J., van der A, R. J., Veefkind, J. P., Stammes, P., Huijnen, V., Kleipool, Q. L., Sneep, M., Claas, J., Leitão, J., Richter, A., Zhou, Y., and Brunner, D.: An improved tropospheric NO_2 column retrieval algorithm for the Ozone Monitoring Instrument, Atmos. Meas. Tech. Discuss., 4, 2329–2388, doi:10.5194/amtd-4-2329-2011, 2011.

Bovensmann, H., Burrows, J. P., Buchwitz, M., Frerick, J., Rozanov, V. V., Chance, K. V., and Goede, A. P. H.: SCIAMACHY: Mission objectives and measurement modes, J. Atmos. Sci., 56, 127–150, doi:10.1175/1520-0469, 1999.

Brinksma, E., Pinardi, G., Braak, R., Volten, H., Richter, A., Schonhardt, A., Van Roozendael, M., Fayt, C., Hermans, C., Dirksen, R., Vlemmix, T., Berkhout, A. J. C., Swart, D. P. J., Oetjen, H., Wittrock, F., Wagner, T., Ibrahim, O., de Leeuw, G., Moerman, M., Curier, L., Celarier, E. A., Knap, W. H., Veefkind, J. P., Eskes, H. J., Allaart, M., Rothe, R., Piters, A. J. M., and Levelt, P.: The 2005 and 2006 DANDELIONS NO_2 and Aerosol Intercomparison Campaigns, J. Geophys. Res., 113, D16S46, doi:10.1029/2007JD008808, 2008.

Bucsela, E. J., Celarier, E. A., Wenig, M. O., Gleason, J. F., Veefkind, J. P., Boersma, K. F., and Brinksma, E.: Algorithm for NO_2 vertical column retrieval from the Ozone Monitoring Instrument, IEEE T. Geosci. Remote Sens., 44(5), 1245–1258, doi:10.1109/TGRS.2005.863715, 2006.

Burrows, J., Weber, M., Buchwitz, M., Rozanov, V., Ladstätter-Weißenmayer, A., Richter, A., Debeek, R., Hoogen, R., Bramstedt, K., Eichmann, K.-U., and Eisinger, M.: The Global Ozone Monitoring Experiment (GOME): Mission concept and first scientific results, J. Atmos. Sci., 56, 151–175, 1999.

Callies, J., Corpaccioli, E., Eisinger, M., Hahne, A., and Lefebvre, A.: GOME-2 – MetOp's Second Generation Sensor for Operational Ozone Monitoring, ESA Bulletin, No. 102, 2000.

Celarier, E. A., Brinksma, E. J., Gleason, J. F., Veefkind, J. P., Cede, A., Herman, J. R., Ionov, D., Goutail, F., Pommereau, J.-P., Lambert, J.-C., van Roozendael, M., Pinardi, G., Wittrock, F., Schönhardt, A., Richter, A., Ibrahim, O. W., Wagner, T., Bojkov, B., Mount, G., Spinei, E., Chen, C. M., Pongetti, T. J., Sander, S. P., Bucsela, E. J., Wenig, M. O., Swart, D. P. J., Volten, H., Kroon, M., and Levelt, P. F.: Validation of Ozone Monitoring Instrument Nitrogen Dioxide Columns, J. Geophys. Res., 113, D15S15, doi:10.1029/2007JD008908, 2008.

CEOS: Data Quality Guidelines for Satellite Sensor Observations Relevant to GEOSS – Calibration and Validation Issues, Recommendations by CEOS/WGCV to the CEOS Task Force, 2004.

Chance, K. V. and Spurr R. J. D.: Ring effect studies: Rayleigh scattering,including molecular parameters for rotational Raman scattering, and the Fraunhofer spectrum, Applied Optics LP, 36(21), 5224–5230, doi:10.1364/AO.36.005224, 1997.

Coldewey-Egbers M., Slijkhuis S., Aberle B., and Loyola, D.: Long-term analysis of GOME in-flight calibration parameters and instrument degradation, Appl. Opt., 47(28), 4749–4761, 2008.

Dikty, S., Richter, A., Bovensmann, H., Wittrock, F., Weber, M., Noël, S., Burrows, J. P., Munro, R., and Lang, R.: GOME-2 level 2 products at IUP Bremen and first results on the quantification of the effects of optical degradation, EUMETSAT Meteorological Satellite Conference, Córdoba, Spain, 20–24 September 2010.

Flemming, J., Inness, A., Flentje, H., Huijnen, V., Moinat, P., Schultz, M. G., and Stein, O.: Coupling global chemistry transport models to ECMWF's integrated forecast system, Geosci. Model Dev., 2, 253–265, doi:10.5194/gmd-2-253-2009, 2009.

Franke, K., Richter, A., Bovensmann, H., Eyring, V., Jöckel, P., Hoor, P., and Burrows, J. P.: Ship emitted NO_2 in the Indian Ocean: comparison of model results with satellite data, Atmos. Chem. Phys., 9, 7289–7301, doi:10.5194/acp-9-7289-2009, 2009.

Gordley, L. L., Russell III, J. M., Mickley, L. J., Frederick, J. E., Park, J. H., Stone, K. A., Beaver, G. M., McInemey, J. M., Deaver, L. E., Toon, G. C., Murcray, F. J., Blatherwick, R. D., Gunson, M. R., Abbatt, J. P. D., Mauldin III, R. L., Mount, G.H., Sen, B., and Blavier, J.-F.: Validation of Nitric Oxide and Nitrogen Dioxide Measurements Made by Halogen Occultation Experiment for UARS Platform, J. Geophys. Res. 101(D6), 10241–10266, doi:10.1029/95JD02143, 1996.

Greenblatt, G. D., Orlando, J. J., Burkholder, J. B., and Ravishankara, A. R.: Absorption measurements of oxygen between 330 and 1140 nm, J. Geophys. Res., 95, 18577–18582, 1990

Gür, B., Spietz, P., Orphal, J., and Burrows, J.: Absorption Spectra Measurements with the GOME-2 FMs using the IUP/IFE-UB's Calibration Apparatus for Trace Gas Absorption Spectroscopy CATGAS, Final Report, IUP University of Bremen, October, 2005.

Heckel, A., Richter, A., Tarsu, T., Wittrock, F., Hak, C., Pundt, I., Junkermann, W., and Burrows, J. P.: MAX-DOAS measurements of formaldehyde in the Po-Valley, Atmos. Chem. Phys., 5, 909–918, doi:10.5194/acp-5-909-2005, 2005.

Heinen, T., Kiemle, S., Buckl, B., Mikusch, E., and Loyola, D.: The Geospatial Service Infrastructure for DLR's National Remote Sensing Data Library, IEEE J. Sel. Top. Appl., 2, 260–269, 2009.

Hollingsworth, A., Engelen, R. J., Textor, C., Benedetti, A., Boucher, O., Chevallier, F., Dethof, A., Elbern, H., Eskes, H., Flemming, J., Granier, C., Kaiser, J. W., Morcrette, J.-J., Rayner, P., Peuch, V.-H., Rouil, L., Schultz, M. G., Simmons, A. J., and the GEMS Consortium: Toward a monitoring and forecasting system for atmospheric composition: The Gems Project. B. Am. Meteorol. Soc., 89, 1147–1164, doi:10.1175/2008BAMS2355.1, 2008.

Hönninger, G., von Friedeburg, C., and Platt, U.: Multi axis differential optical absorption spectroscopy (MAX-DOAS), Atmos. Chem. Phys., 4, 231–254, doi:10.5194/acp-4-231-2004, 2004.

Horowitz, L., Walters, S., Mauzerall, D., Emmons, L., Rasch, P., Granier, C., Tie, X., Lamarque, J., Schultz, M., Tyndall, G., Orlando, J., and Brasseur, G.: A global simulation of tropospheric ozone and related tracers: description and evaluation of MOZART, version 2, J. Geophys. Res., 108(D24), 4784, doi:10.1029/2002JD002853, 2003.

Irie, H., Kanaya, Y., Akimoto, H., Tanimoto, H., Wang, Z., Gleason, J. F., and Bucsela, E. J.: Validation of OMI tropospheric NO_2 column data using MAX-DOAS measurements deep inside the North China Plain in June 2006: Mount Tai Experiment 2006, Atmos. Chem. Phys., 8, 6577–6586, doi:10.5194/acp-8-6577-2008, 2008.

Ionov, D. V., Timofeyev, Y. M., Sinyakov, V. P., Semenov, V. K., Goutail, F., Pommereau, J.-P., Bucsela, E. J., Celarier, E. A., and Kroon, M.: Ground-based validation of EOS-Aura OMI NO_2 vertical column data in the midlatitude mountain ranges of Tien Shan (Kyrgyzstan) and Alps (France), J. Geophys. Res., 113, D15S08, doi:10.1029/2007JD008659, 2008.

Jacob, D. J., Heikes, E. G., Fan, S.-M., Logan, J. A., Mauzerall, D. L., Bradshaw, J. D., Singh, H. B., Gregory, G. L., Talbot, R. W., Blake, D. R., and Sachse, G. W.: Origin of ozone and NO_x in the tropical troposphere: A photochemical analysis of aircraft observations over the South Atlantic basin, J. Geophys. Res., 101, 24235–24250, 1996.

Kleinpool, Q. L., Dobber, M. R., de Haan, J. F., and Levelt, P. F.: Earth surface reflectance climatology from 3 years of OMI data, J. Geophys. Res, 113, D18308, doi:10.1029/2008JD010290, 2008.

Konovalov, I. B., Beekmann, M., Richter, A., Burrows, J. P., and Hilboll, A.: Multi-annual changes of NO_x emissions in megacity regions: nonlinear trend analysis of satellite measurement based estimates, Atmos. Chem. Phys., 10, 8481–8498, doi:10.5194/acp-10-8481-2010, 2010.

Kurylo, M. J. and Zander, R. J.: The NDSC – Its status after ten years of operation, in: Proceedings of the Quadrennial Ozone Symposium, edited by: Bojikov, R. D. and Kazuo, S., Sapporo, Japan, 2–8 July 2000, 137–138, 2000.

Lambert, J.-C. and Balis, D.: Delta validation report for ERS-2 GOME Data Processor Upgrade to Version 4.0. ERSE-CLVL-EOPG-TN-04-0001, ESA/ESRIN, Frascati, Italy, 2004.

Lambert, J. C., Granville, J., Van Roozendael, M., Sarkissian, A., Goutail, F., Müller, J.-F., Pommereau, J.-P., and Russell III, J. M.: A climatology of NO_2 profile for improved air mass factors for ground-based vertical column measurements, Proceedings of the 5th European Symposium Strat. Ozone, Saint Jean de Luz, September 1999, Air pollution research report 73, European

Commission, edited by: Harris NRP, Guirlet M, Amanatidis GT, p. 703, ISBN 92-827-5672-6, 2000.

Lambert, J.-C., Granville, J., Soebijanta, V., and Van Roozendael, M.: Geophysical Validation of GOME GDP 3.0 Total NO_2. In: ERS-2 GOME GDP 3.0 Implementation and Delta Validation, Validation Report for GOME Level 1-to-2 Data Processor Upgrade to Version GDP 3.0, edited by: Lambert, J.-C., ERSE-DTEX-EOAD-TN-02-0006, ESA/ESRIN, Frascati, Italy, 2002.

Lambert, J.-C., Blumenstock, T., Boersma, F., Bracher, A., De Mazière, M., Demoulin, P., De Smedt, I., Eskes, H., Gil, M., Goutail, F., Granville, J., Hendrick, F., Ionov, D. V., Johnston, P. V., Kostadinov, I., Kreher, K., Kyrö, E., Martin, R., Meier, A., Navarro-Comas, M., Petritoli, A., Pommereau, J.-P., Richter, A., Roscoe, H. K., Sioris, C., Sussmann, R.,Van Roozendael, M., Wagner, T., Wood, S., and Yela, M.: Geophysical Validation of SCIAMACHY NO_2 Vertical columns: Overview of Early 2004 Results. Proceedings of the Second Workshop on the Atmospheric Chemistry Validation of ENVISAT (ACVE-2), 3–7 May 2004, ESA-ESRIN, Frascati, Italy (ESA SP-562), edited by: Danesy, D., 6.1–6.13, 2004.

Lambert, J.-C., Pinardi, G., Hao, N., and Valks, P.: GOME-2 GDP 4.2 total NO_2 (NTO/OTO) validation update and tropospheric NO_2 validation set-up, TN-IASB-GOME2-O3MSAF-NO2-02_ORR-B_1, 24 November, 2008.

Lambert, J.-C. et al.: Atmospheric Monitoring Services – Stage 2 of the Earthwatch GMES Services Element, PROMOTE-2, C5 Service Validation Protocol, Version 3, October, 2009.

Lang, R., Munro, R., Livschitz, Y., Dyer, R., and Lacan, A.: GOME-2 FM3 Long-Term In-Orbit Degradation – Basic Signatures After 2nd Throughput Test, EUMETSAT Technical report, EUM.OPS-EPS.DOC.09.0464, 2009.

Leitão, J., Richter, A., Vrekoussis, M., Kokhanovsky, A., Zhang, Q. J., Beekmann, M., and Burrows, J. P.: On the improvement of NO_2 satellite retrievals - aerosol impact on the airmass factors, Atmos. Meas. Tech., 3, 475–493, doi:10.5194/amt-3-475-2010, 2010.

Leue, C., Wenig, M., Wagner, T., Klimm, O., Platt, U., and Jähne, B.: Quantitative analysis of NOx emissions from Global Ozone Monitoring Experiment satellite image sequences, J. Geophys. Res., 106, 5493–5505, 2001.

Levelt, P. F., van den Oord, G. H. J., Dobber, M. R., Mälkki, A., Visser, H., de Vries, J., Stammes, P., Lundell, J. O. V., and Saari, H.: The Ozone Monitoring Instrument, IEEE T. Geosci. Remote Sens., 44(5), 1093–1101, doi:10.1109/TGRS.2006.872333, 2006.

Livschitz, Y. and Loyola, D.: Design Document for the GOME-2 Universal Processor for Atmospheric Spectrometers, SAF/O3M/DLR/DD/001, Issue 2.0, October, 2003.

Loyola, D., Thomas, W., Livschitz, Y., Ruppert, T., Albert, P., and Hollmann, R.: Cloud properties derived from GOME/ERS-2 backscatter data for trace gas retrieval, IEEE T. Geosci. Remote Sens., 45(9), 2747–2758, 2007.

Loyola, D., Koukouli, M. E., Valks, P., Balis, D. S., Hao, N., Van Roozendael, M., Spurr, R. J. D., Zimmer, W., Kiemle, S., Lerot, C., and Lambert, J.-C.: The GOME-2 Total Column Ozone Product: Retrieval Algorithm and Ground-Based Validation, J. Geophys. Res., 116, D07302, doi:10.1029/2010JD014675, 2011.

Martin, R. V., Chance, K., Jacob, D. J., Kurosu, T. P., Spurr, R. J. D., Bucsela, E., Gleason, J. F., Palmer, P. I., Bey, I., Fiore, A. M., Li, Q., Yantosca, R. M., and Koelemeijer, R. B. A.: An improved retrieval of tropospheric nitrogen dioxide from GOME, J. Geophys. Res., 107(D20), 4437, doi:10.1029/2001JD001027, 2002.

Munro, R., Eisinger, M., Anderson, C., Callies, J., Corpaccioli, E., Lang, R., Lefebvre, A., Livschitz, Y., and Perez Albinana, A.: GOME-2 on MetOp: From in-orbit verification to routine operations, in: Proceedings of EUMETSAT Meteorological Satellite Conference, Helsinki, Finland, 12–16 June 2006.

Nüß, H., Richter, A., Valks, P., and Burrows, J.: Improvement of the NO_2 total column retrieval for GOME-2, O3M-SAF Visiting Scientist Report, IUP University of Bremen, available at: http://o3msaf.fmi.fi, November, 2006.

Palmer, P. I., Jacob, D. J., Chance, K., Martin, R. V., Spurr, R. J. D., Kurosu, T. P., Bey, I., Yantosca, R., Fiore, A., and Li, Q.: Airmass factor formulation for spectroscopic measurements from satellites: application to formaldehyde retrievals from GOME, J. Geophys. Res., 106, 14539–14550, 2001.

Pinardi, G., Hendrick, F., Clémer, K., Lambert, J. C., Bai, J., and Van Roozendael, M.: On the use of the MAXDOAS technique for the validation of tropospheric NO_2 column measurements from satellite, proceeding of the EUMETSAT Meteorological Satellite Conference, 9–12 September 2008, Darmstadt, Germany, 2008.

Platt, U.: Differential optical absorption spectroscopy (DOAS), in Air Monitoring by Spectroscopic Techniques, Chem. Anal. Ser., 127, 27–84, John Wiley, New York, 27–84, 1994.

Platt, U. and Stutz, J.: Differential Optical Absorption Spectroscopy, Principles and Applications, Springer, Physics of Earth and Space Environments, ISBN 978-3-540-21193-8, 2008.

Popp, C., Wang, P., Brunner, D., Stammes, P., Zhou, Y., and Grzegorski, M.: MERIS albedo climatology for FRESCO+ O_2 A-band cloud retrieval, Atmos. Meas. Tech., 4, 463–483, doi:10.5194/amt-4-463-2011, 2011.

Randall, C. E., Rusch, D. W., Bevilacqua, R. M., Hoppel, K. W., and Lumpe, J. D.: Polar Ozone and Aerosol Measurements (POAM) II Stratospheric NO_2, 1993-1996, J. Geophys. Res., 103, 28361–28371, 1998.

Richter, A. and Burrows, J.: Tropospheric NO_2 from GOME measurements, Adv. Space Res., 29, 1673–1683, 2002.

Richter, A. and Wagner, T.: Diffuser plate spectral structures and their influence on GOME slant columns, Technical note, available at: www.iup.uni-bremen.de/gome/data/diffuser_gome.pdf, 2001.

Richter, A., Eyring, V., Burrows, J., Bovensmann, H., Lauer, A., Sierk, B., and Crutzen, P.: Satellite measurements of NO_2 from international shipping emissions, Geophys. Res. Lett., 31, L23110, doi:10.1029/2004GL020822, 2004

Richter, A., Burrows, J. P., Nüß, H., Granier, C., and Niemeier, U.: Increase in tropospheric nitrogen dioxide over China observed from space, Nature, 437, 129–132, 2005.

Richter, A., Begoin, M., Hilboll, A., and Burrows, J. P.: An improved NO_2 retrieval for the GOME-2 satellite instrument, Atmos. Meas. Tech., 4, 1147–1159, doi:10.5194/amt-4-1147-2011, 2011.

Roscoe, H. K., Van Roozendael, M., Fayt, C., du Piesanie, A., Abuhassan, N., Adams, C., Akrami, M., Cede, A., Chong, J., Clémer, K., Friess, U., Gil Ojeda, M., Goutail, F., Graves, R., Griesfeller, A., Grossmann, K., Hemerijckx, G., Hendrick, F.,

Herman, J., Hermans, C., Irie, H., Johnston, P. V., Kanaya, Y., Kreher, K., Leigh, R., Merlaud, A., Mount, G. H., Navarro, M., Oetjen, H., Pazmino, A., Perez-Camacho, M., Peters, E., Pinardi, G., Puentedura, O., Richter, A., Schönhardt, A., Shaiganfar, R., Spinei, E., Strong, K., Takashima, H., Vlemmix, T., Vrekoussis, M., Wagner, T., Wittrock, F., Yela, M., Yilmaz, S., Boersma, F., Hains, J., Kroon, M., Piters, A., and Kim, Y. J.: Intercomparison of slant column measurements of NO_2 and O_4 by MAX-DOAS and zenith-sky UV and visible spectrometers, Atmos. Meas. Tech., 3, 1629–1646, doi:10.5194/amt-3-1629-2010, 2010.

Rothman, L. S., Barbe, A., Chris Benner, D., Brown, L. R., Camy-Peyret, C., Carleer, M. R., Chance, K., Clerbaux, C., Dana, V., Devi, V. M., Fayt, A., Flaud, J.-M., Gamache, R. R., Goldman, A., Jacquemart, D., Jucks, K. W., Lafferty, W. J., Mandin, J.-Y., Massie, S. T., Nemtchinov, V., Newnham, D. A., Perrin, A., Rinsland, C. P., Schroeder, J., Smith, K. M., Smith, M. A. H., Tang, K., Toth, R. A., Vander Auwera, J., Varanasi, P., and Yoshino, K.: The HITRAN molecular spectroscopic database: edition of 2000 including updates through 2001, J. Quant. Spectrosc. Radiat. Transfer, 82, 5–44, 2003.

Seinfeld, J. H. and Pandis, S. N.: Atmospheric Chemistry and Physics, from Air Pollution to Climate Change, John Wiley, New York, 1326 pp., ISBN 0-471-17815-2, 1998.

Solomon, S.: Stratospheric ozone depletion: A review of concepts and history, Rev. Geophys., 37(3), 275–316, 1999.

Spurr, R.: LIDORT and VLIDORT: Linearized pseudo-spherical scalar and vector discrete ordiate radiative transfer models for use in remote sensing retrieval problems. Light Scattering Reviews, Volume 3, edited by: Kokhanovsky, A., Springer, 2008.

Spurr, R. J. D., Kurosu, T. P., and Chance, K. V.: A Linearized discrete Ordinate Radiative Transfer Model for Atmospheric Remote Sensing Retrieval, J. Quant. Spectrosc. Radiat. Transfer, 68, 689–735, 2001.

Spurr, R., Zimmer, W., Loyola, D., Coldewey-Egbers, M., Lerot, C., Van Roozendael, M., Lambert, J.-C., Granville, J., Koukouli, M., and Balis, D.: Clouds as Scattering Layers: Improved Retrieval of GOME-2 Total Column Products, in: Proceedings of EUMETSAT Meteorological Satellite Conference, Bath, UK, 21–25 September, 2009.

Valks, P., Loyola, D., Hao, N., Rix, M., and Slijkhuis, S.: Algorithm Theoretical Basis Document for GOME-2 Total Column Products of Ozone, Minor Trace Gases and Cloud Properties (GDP 4.4 for O3M-SAF OTO and NTO), DLR/GOME-2/ATBD/01, Iss./Rev.: 2/D, available at: http://o3msaf.fmi.fi, January, 2011.

Vandaele, A. C., Hermans, C., Simon, P. C., Carleer, M., Colin, R., Fally, S., Merienne, M. F., Jenouvrier, A., and Coquart, B.: Measurements of the NO_2 absorption cross-section from 42000 cm-1 to 10000 cm-1 (238-1000 nm) at 220 K and 294 K, J. Quant. Spectrosc. Radiat. Transfer, 59, 171–184, 1998.

Van der A, R. J., Peters, D. H. M. U., Eskes, H., Boersma, K. F., Van Roozendael, M., De Smedt, I., and Kelder, H. M.: Detection of the trend and seasonal variation in tropospheric NO_2 over China, J. Geophys. Res., 111, D12317, doi:10.1029/2005JD006594, 2006.

Van der A, R. J., Eskes, H. J., Boersma, K. F., van Noije, T. P. C., Van Roozendael, M., De Smedt, I., Peters, D. H. M. U., and Meijer, E. W.: Trends, seasonal variability and dominant NO_x source derived from a ten year record of NO_2 measured from space, J. Geophys. Res., 113, D04302, doi:10.1029/2007JD009021, 2008.

Velders, G. J. M., Granier, C., Portmann, R. W., Pfeilsticker, K., Wenig, M., Wagner, T., Platt, U., Richter, A., and Burrows, J. P.: Global tropospheric NO_2 column distributions: Comparing three-dimensional model calculations with GOME measurements, J. Geophys. Res., 106, 12643–12660, 2001.

Wagner, T., Dix, B., Friedburg, C. v., Frieß, U., Sanghavi, S., Sinreich, R., and Platt, U.: MAX-DOAS O_4 measurements: A new technique to derive information on atmospheric aerosols- Principles and information content, J. Geophys. Res., 109, D22205, doi:10.1029/2004JD004904, 2004.

Wenig, M., Kühl, S., Beirle, S., Bucsela, E., Jähne, B., Platt, U., Gleason, J., and Wagner, T.: Retrieval and analysis of stratospheric NO_2 from the Global Ozone Monitoring Experiment, J. Geophys. Res., 109, D04315, doi:10.1029/2003JD003652, 2004.

Wittrock, F., Oetjen, H., Richter, A., Fietkau, S., Medeke, T., Rozanov, A., and Burrows, J. P.: MAX-DOAS measurements of atmospheric trace gases in Ny-Ålesund – Radiative transfer studies and their application, Atmos. Chem. Phys., 4, 955–966, doi:10.5194/acp-4-955-2004, 2004.

Zhou, Y., Brunner, D., Boersma, K. F., Dirksen, R., and Wang, P.: An improved tropospheric NO_2 retrieval for OMI observations in the vicinity of mountainous terrain, Atmos. Meas. Tech., 2, 401–416, doi:10.5194/amt-2-401-2009, 2009.